AD—A114 336   NATIONAL OCEANIC AND ATMOSPHERIC ADMINISTRATION BOUL—ETC F/G 20/5
                OPTICAL AND IN SITU MEASURING OF STRUCTURE PARAMETERS RELEVANT —ETC(U)
                MAR 82   W KOHSIEK
UNCLASSIFIED   NOAA—TM—ERL—WPL—96   ARO-18029.2-GS   NL

END
DATE
FILMED
6-82
DTIC

NOAA-Technical Memorandum-ERL-WPL-96

OPTICAL AND IN SITU MEASURING OF STRUCTURE PARAMETERS
RELEVANT TO TEMPERATURE AND HUMIDITY, AND THEIR APPLICATION
TO THE MEASURING OF SENSIBLE AND LATENT HEAT FLUX

W. Kohsiek
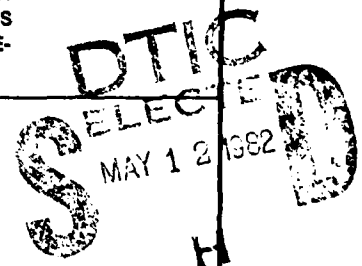
Wave Propagation Laboratory
Boulder, Colorado
March 1982

noaa NATIONAL OCEANIC AND
ATMOSPHERIC ADMINISTRATION / Environmental Research
Laboratories

REPORT DOCUMENTATION PAGE		READ INSTRUCTIONS BEFORE COMPLETING FORM
1. REPORT NUMBER	2. GOVT ACCESSION NO.	3. RECIPIENT'S CATALOG NUMBER
4. TITLE (and Subtitle) OPTICAL AND IN SITU MEASURING OF STRUCTURE PARAMETERS RELEVANT TO TEMPERATURE AND HUMIDITY, AND THEIR APPLICATION TO THE MEASURING OF SENSIBLE AND LATENT HEAT FLUX		5. TYPE OF REPORT & PERIOD COVERED
		6. PERFORMING ORG. REPORT NUMBER
7. AUTHOR(s) W. Kohsiek		8. CONTRACT OR GRANT NUMBER(s) ARO 55-81
9. PERFORMING ORGANIZATION NAME AND ADDRESS National Oceanic and Atmospheric Administration Environmental Research Laboratories Boulder, Colorado 80303		10. PROGRAM ELEMENT, PROJECT, TASK AREA & WORK UNIT NUMBERS
11. CONTROLLING OFFICE NAME AND ADDRESS U. S. Army Research Office Post Office Box 12211 Research Triangle Park, NC 27709		12. REPORT DATE March 1982
		13. NUMBER OF PAGES 64
14. MONITORING AGENCY NAME & ADDRESS(if different from Controlling Office)		15. SECURITY CLASS. (of this report) Unclassified
		15a. DECLASSIFICATION/DOWNGRADING SCHEDULE

16. DISTRIBUTION STATEMENT (of this Report)

Approved for public release; distribution unlimited.

17. DISTRIBUTION STATEMENT (of the abstract entered in Block 20, if different from Report)

18. SUPPLEMENTARY NOTES

THE VIEW, OPINIONS AND/OR FINDINGS CONTAINED IN THIS REPORT ARE THOSE OF THE AUTHOR(S) AND SHOULD NOT BE CONSTRUED AS AN OFFICIAL DEPARTMENT OF THE ARMY POSITION, POLICY, OR DE-CISION, UNLESS SO DESIGNATED BY OTHER DOCUMENTATION.

19. KEY WORDS (Continue on reverse side if necessary and identify by block number)

1. Optics
2. Refractive Turbulence
3. Heat Flux
4. Remote Sensing
5. Humidity Fluctuations

20. ABSTRACT (Continue on reverse side if necessary and identify by block number)

Optical measurements of the structure parameters of temperature (C_T^2), humidity (C_Q^2) and temperature-humidity (C_{TQ}) were attempted at 0.94 μm, 10.7 μm (CO_2 laser) and 337 μm (HCN laser), but owing to various instrumental problems no measurement of C_Q^2 and C_{TQ} could be achieved.

In situ measurements of the same parameters were more successful. Two

DD FORM 1473 1 JAN 73   EDITION OF 1 NOV 65 IS OBSOLETE   UNCLASSIFIED

techniques of measuring structure parameters are compared: by using spaced sensors, and by time-lagging one sensor. In this way the expected $r^{2/3}$ dependency of the structure parameter could be checked (r = distance between sensors, either by spacing or by time-lagging). From the connection between structure parameters and spectra, evidence of an inertial subrange for the temperature-humidity cospectrum is found. Special attention is paid to the use of Ly-α hygrometry for measuring structure parameters involving humidity. Finally, relations between the structure parameters C_T^2 and C_Q^2, and the fluxes of heat and moisture are discussed; an effect of atmospheric stability was not detectable for $-z/L > 0.02$.

Accession For

NTIS GRA&I	☑	
DTIC TAB	☐	
Unannounced	☐	
Justification		

By

Distribution/

Availability Codes

Dist	Avail and/or Special
A	

NOAA Technical Memorandum ERL WPL-96

OPTICAL AND IN SITU MEASURING OF STRUCTURE PARAMETERS
RELEVANT TO TEMPERATURE AND HUMIDITY, AND THEIR APPLICATION
TO THE MEASURING OF SENSIBLE AND LATENT HEAT FLUX

W. Kohsiek

Wave Propagation Laboratory
Boulder, Colorado
March 1982

NOTICE

CONTENTS

OPTICAL AND IN SITU MEASURING OF STRUCTURE PARAMETERS RELEVANT TO TEMPERATURE AND HUMIDITY, AND THEIR APPLICATION TO THE MEASURING OF SENSIBLE AND LATENT HEAT FLUX

W. Kohsiek[1]

ABSTRACT

Optical measurements of the structure parameters of temperature $(C_T^{\ 2})$, humidity $(C_Q^{\ 2})$ and temperature-humidity (C_{TQ}) were attempted at 0.94 μm, 10.7 μm (CO_2 laser) and 337 μm (HCN laser), but owing to various instrumental problems no measurement of $C_Q^{\ 2}$ and C_{TQ} could be achieved. In situ measurements of the same parameters were more successful. Two techniques of measuring structure parameters are compared: by using spaced sensors, and by time-lagging one sensor. In this way the expected $r^{2/3}$ dependency of the structure parameter could be checked (r = distance between sensors, either by spacing or by time-lagging). From the connection between structure parameters and spectra, evidence of an inertial subrange for the temperature-humidity cospectrum is found. Special attention is paid to the use of Ly-α hygrometry for measuring structure parameters involving humidity. Finally, relations between the structure parameters $C_T^{\ 2}$ and $C_Q^{\ 2}$, and the fluxes of heat and moisture are discussed; an effect of atmospheric stability was not detectable for $-z/L > 0.02$.

1. INTRODUCTION

The effect of atmospheric turbulence on propagation of electromagnetic radiation in the atmosphere has received renewed interest in the last two decades, mainly because of its degrading effect on optical communications. For the meteorologist, however, this very degradation provides a means for studying atmospheric

---

[1] Koninklijk Nederlands Meteorologisch Instituut
3730 AE DE BILT
The Netherlands

turbulence. In particular, by observing the scintillation of a visible light beam one can infer the temperature structure parameter C_T^2, defined by

$$C_T^2 = \frac{<(T_A - T_B)^2>}{r_{AB}^{2/3}} \, , \qquad (1)$$

where $T_A - T_B$ is the temperature difference between two close locations A and B, and r_{AB} is the distance A-B. The brackets indicate an ensemble average. The locations A and B should be so close that any temperature difference can result only from inertial-subrange turbulent structures (Wyngaard, 1973). The quantity $<(T_A - T_B)^2>$ is called the temperature structure function, and denoted by $D_T(r)$.

The temperature structure parameter is one of the parameters describing the state of the atmospheric boundary layer. Its magnitude is related to the sensible heat flux at the Earth's surface. In the case of a very unstable atmosphere, the relation has the simple form of

$$H = 0.806 \, \rho \, c_p z \, (C_T^2)^{3/4} \, (\frac{kg}{T})^{1/2}, \qquad (2)$$

where H is the sensible heat flux (W m^{-2}), ρ the air density (kg m^{-3}), c_p the specific heat of air at constant pressure (J kg^{-1} K^{-1}), z the height above the surface (m), k the von Kármán constant, g the acceleration of gravity (m s^{-2}) and T the absolute temperature (K). C_T^2 has dimensions K^2 m$^{-2/3}$. For less unstable situations, the relation is more complex and involves a stability parameter (Wyngaard and Clifford, 1978).

Similar to the above expression, a relation has been proposed connecting the humidity structure parameter to the evaporation or latent heat flux:

$$LE_o = 0.806 \, L \, z \, (C_T^2)^{1/4} \, (C_Q^2)^{1/2} \, (\frac{kg}{T})^{1/2} \, , \qquad (3)$$

where LE_o is the latent heat flux (W m^{-2}), L the latent heat of evaporation (J kg^{-1}) and C_Q^2 the humidity structure parameter defined as

$$C_Q^2 = \frac{<(Q_A - Q_B)^2>}{r_{AB}^{2/3}} \, . \qquad (4)$$

2

In this report we express the humidity Q in kg m^{-3}, so C_Q^2 has dimension kg^2 m^{-6} m$^{-2/3}$.

Relation (2) has been explored in the past to some extent (e.g., Wyngaard et al., 1978; Davidson et al., 1978; Coulter and Wesely, 1980), but experimental data to test relation (3) are more scarce (Farrall et al., 1980).

The link between structure parameters and optical propagation becomes obvious if one considers the expression for the scintillation of a spherical wave of light along a horizontal path (e.g., Wang et al., 1978):

$$\sigma_\chi^2 = 0.124 \ k^{7/6} \ L^{11/6} \ C_n^2 \ , \tag{5}$$

$$C_n^2 = A_T^2 \ C_T^2/{<T>}^2 + A_Q^2 \ C_Q^2/{<Q>}^2 + 2A_T A_Q \ C_{TQ}/{<T><Q>} \ . \tag{6}$$

The relation (5) is valid for the case of a spherical wavefront, infinitesimally small receiver aperture, and inertial subrange fluctuations. σ_χ^2 is the variance of the log-amplitude of the received light, k is the wavenumber (k = $2\pi/\lambda$) expressed in m^{-1}, L the path length between transmitter and receiver (m). The coefficients A_T and A_Q depend on wavelength, humidity, temperature, and pressure, and C_{TQ} is the temperature-humidity structure parameter defined by

$$C_{TQ} = \frac{<(T_A - T_B)(Q_A - Q_B)>}{r_{AB}^{2/3}} \ . \tag{7}$$

C_n^2 is the refractive index structure parameter. The first term on the right-hand side of (6) gives the effect of temperature fluctuations on the scintillation, the second term that of humidity fluctuations and the third term the effect of correlated temperature-humidity fluctuations. The first two terms are always positive, whereas the third term can have either sign.

The quantities A_T and A_Q can be calculated from a knowledge of air pressure, temperature, humidity, and the line strengths and shapes of water vapor absorption lines. The effect of other gases, like CO_2, may usually be neglected. An extensive calculation of A_T and A_Q, and of other quantities referring to optical propagation has been performed by Hill et al. (1980) for the wavelength interval 4.7 μm to radio wavelengths.

3

For the three wavelengths of interest (0.94 μm, 10.7 μm, and 337 μm) it is useful to have analytic expressions for A_T and A_Q so that their values can be obtained easily for the given mean temperature, humidity, and pressure during a measurement. These quantities were calculated (by R.J. Hill and J.T. Priestley) over a range of temperatures from -10°C to 38°C, for relative humidities from 0% to 100%, and pressures 810 to 1060 mbar. The resulting calculated values were fitted to simple functional forms (by R.S. Lawrence). The values of A_T and A_Q are essentially the same at 0.94 μm as for visible light; thus

$$A_T(0.94 \text{ μm}) = -77.49 \text{ PT} \times 10^{-6}$$

and
$$A_Q(0.94 \text{ um}) = -59.00 \text{ Q} \times 10^{-6} ,$$

where P is total atmospheric pressure in mbar, T is temperature in Kelvin, and Q is the water vapor density in kg m^{-3}. For 10.7 μm the functional fit gave

$$A_T(10.7 \text{ μm}) = A_T(0.94 \text{ μm}) - 2.5 \times 10^{-23} (T_c + 91)^{7.487} R$$

and
$$A_Q(10.7 \text{ μm}) = A_Q(10.7 \text{ μm}) - 4.172 \times 10^{-19} (T_c + 86)^{6.22} R ,$$

where T_c is temperature in Celsius and R is the fractional relative humidity. For 337 μm the functional fit gave

$$A_T(337 \text{ μm}) = A_T(0.94 \text{ μm}) - (34.54 + 2.325 T_c + 0.0626 T_c^2 + 0.001527 T_c^3) R \times 10^{-6}$$

and

$$A_Q(337 \text{ μm}) = A_Q(0.94 \text{ μm}) + (35.26 + 2.353 T_c + 0.06247 T_c^2 + 0.00151 T_c^3) R \times 10^{-6} .$$

For reasons of convenience, we rewrite (5) and (6) as

$$\sigma_\chi^2 = .124 \, k^{7/6} L^{11/6} \frac{A_Q^2 C_Q^2}{<Q>^2} \left[\frac{A_T^2/<T>^2}{A_Q^2/<Q>^2} \frac{C_T^2}{C_Q^2} + 1 + 2 \frac{A_T/<T>}{A_Q/<Q>} \frac{C_{TQ}}{C_Q^2} \right] , \quad (8)$$

4

and illustrate with an example how temperature, humidity, and their correlation contribute to the scintillation. We put $\langle T \rangle$ = 298 K, $\langle Q \rangle = 10^{-2}$ kg m^{-3} (which implies a relative humidity of 40%), $C_T^{\,2}$ = 0.367 K^2 m$^{-2/3}$ (corresponding, using (2) with z = 4 m, to a sensible heat flux of 200 W m^{-2}), and $C_Q^{\,2} = 0.367 \times 10^{-6}$ kg^2 m^{-6} m$^{-2/3}$ (a latent heat flux of about 400 W m^{-2}, using (3)). We consider three wavelengths: 0.94 μm, 10.7 μm, and 337 μm. Finally, we assume a perfect positive correlation between temperature and humidity fluctuations, consequently $C_{TQ} = (C_T^{\,2} C_Q^{\,2})^{1/2}$. The values of the three quantities between the square brackets in (8) are given in Table 1. Only for the longest wavelength considered (337 μm), is the effect of temperature fluctuations small, whereas at 10.7 μm both temperature and temperature-humidity effects have importance and at 0.94 μm temperature fluctuations are dominant. This observation leads to the original goal of the present work: by measuring the scintillation at these three wavelengths it should be possible to obtain three equations with three unknowns, $C_T^{\,2}$, $C_Q^{\,2}$, and C_{TQ}. Solving these equations for the structure parameters, and applying relations (2) and (3), would lead to the fluxes of sensible and latent heat.

Of course, in practice it is not as simple as that. First, there are instrumental limitations. These are discussed in Section 2. A second limitation is set by the ratio C_T/C_Q. If this ratio is several times larger than the value assumed in the above example, the temperature effect will dominate at both 0.94 and 10.7 μm, thus making the set of equations non-unique. This is likely to occur

Table 1.--Scintillation parameters at $\langle T \rangle$ = 298 K, $\langle Q \rangle = 10^{-2}$ kg m^{-3}, $C_T^{\,2}$ = 0.367 K^2 m$^{-2/3}$, $C_Q^{\,2} = 0.367 \times 10^{-6}$ kg^2 m^{-6} m$^{-2/3}$.

λ(μm)	Effect of temperature	Effect of humidity	Effect of temperature-humidity	Transmission 200 m	A_T	A_Q
0.94	286	1	34	0.90*	-2.62×10^{-4}	-5.79×10^{-7}
10.7	22	1	9.4	0.96	-2.16×10^{-4}	-1.55×10^{-6}
337	0.016	1	-0.26	0.05	-2.84×10^{-4}	7.43×10^{-5}

* From an unpublished calculation of Lawrence and Ochs.

if the evaporation rate is severely limited by the lack of soil moisture, a situation often encountered in the non-irrigated parts of eastern Colorado.

From (2) and (3), one immediately infers that $C_T/C_Q = H/LE_0 \times L/\mu c_p \approx 2.5 \times 10^3 \beta$, where $\beta = H/LE_0$ is the Bowen ratio. The relation between C_T^2/C_Q^2 and β has been pointed out earlier by Wesely (1976). A Bowen ratio of 0.5, like the one assumed in the example, is characteristic of a freely evaporating vegetation. If the water supply is restricted, $\beta > 1$ is more likely. If the ratio C_T/C_Q is very small, as may occur above a water surface, humidity fluctuations may be dominant in the far infrared, and even contribute to the scintillation at visible wavelengths. Finally, the correlation between temperature and humidity fluctuations adds to the variety of possible cases. This has been discussed in detail by Wesely (1976). A strong effect of humidity fluctuations on the refractive index was observed by Friehe et al. (1975).

2. SCINTILLATION MEASUREMENTS--INSTRUMENTS AND RESULTS

2.1 General Features of the Three Scintillometers

Instrumental parameters of the three scintillometers we used are summarized in Table 2. Of the available suitable infrared light sources, we decided to use a CO_2 laser (10.7 μm) and an HCN laser (337 μm). The 0.94 μm scintillometer has a LED light source. As discussed in the foregoing, we expected that each of the three contributions to the refractive-index fluctuations (temperature fluctuations,

Table 2.--Instrument parameters of the three scintillometers.

λ (μm)	Diameter transmitter (m)	Diameter receiver (m)	Output power (mW)	Modulation frequency (Hz)	Divergence transmitter (mrad)	Divergence receiver (mrad)	Fresnel zone (m)
0.94	0.05	0.05	20	25000	6	*	0.0137
10.7	0.002	0.05	3000	260	10	8	0.046
337	0.03	0.25	30	150	10	12	0.26

* The detector is positioned in the exit pupil of a binocular optics.

humidity fluctuations, and correlated temperature-humidity fluctuations) should be prominent in one of the scintillometers.

The scintillometers were operated on Table Mountain over a path of 200 m at a height of 4 m. The path length was the result of a trade-off between the absorption of the 337 μm radiation (see Table 1) and the strength of the scintillation (increasing with path length, see Eq. (5)). The height was such that no outer-scale effects were anticipated (e.g., Hill and Ochs, 1978). Since the scintillation σ_χ^2 decreases with height (Wyngaard and Clifford, 1978), it is wise to choose the path height as low as possible, giving consideration to outer-scale effects. Table Mountain is a flat and uniform terrain about 10 miles north of Boulder. The "mountain" is about 50 m higher than its surroundings and is covered with a sparse vegetation of grass. The scintillometers were set up near the optical building, in an approximately N-S orientation with the detectors south, about 10 m from the building, on top of a tripod (Fig. 1). The transmitters were housed inside and on top of a trailer. In Fig. 2 the position of the scintillometers and that of other instruments is indicated.

The output of the transmitters was modulated for better discrimination against low-frequency background fluctuations; besides, the pyroelectric detectors used for the CO_2 and HCN scintillometer are only sensitive to irradiation changes. The modulation frequencies of 260 Hz (10.7 μm) and 150 Hz (337 μm) were chosen on considerations of the high-frequency roll-off of the detectors signal bandwidth, mutual interference, and 60-Hz interference. The 0.94 μm LED scintillometer can be operated on a much higher modulation frequency (25 kHz) because of different detector characteristics. Each detector unit has two circular apertures and two detector cells. The receiver apertures of the CO_2 and HCN scintillometers were tangent; those of the LED scintillometer were not. Besides the advantage of a better rejection of large eddy sizes (Wang et al., 1978), taking the difference of signals from two receiving apertures provides compensation for 60-Hz pickup, and for light source and background fluctuations. For the CO_2 and the HCN scintillometers pyroelectric detectors were used because they are easy to handle (no cooling required) and provide sufficient sensitivity for our purpose (at least, in theory).

As the arrangement of the scintillometers differs from a point source/point detector setup, the expression relating the scintillation to the structure parameters differs from (5) by a factor depending on the geometry of the apertures.
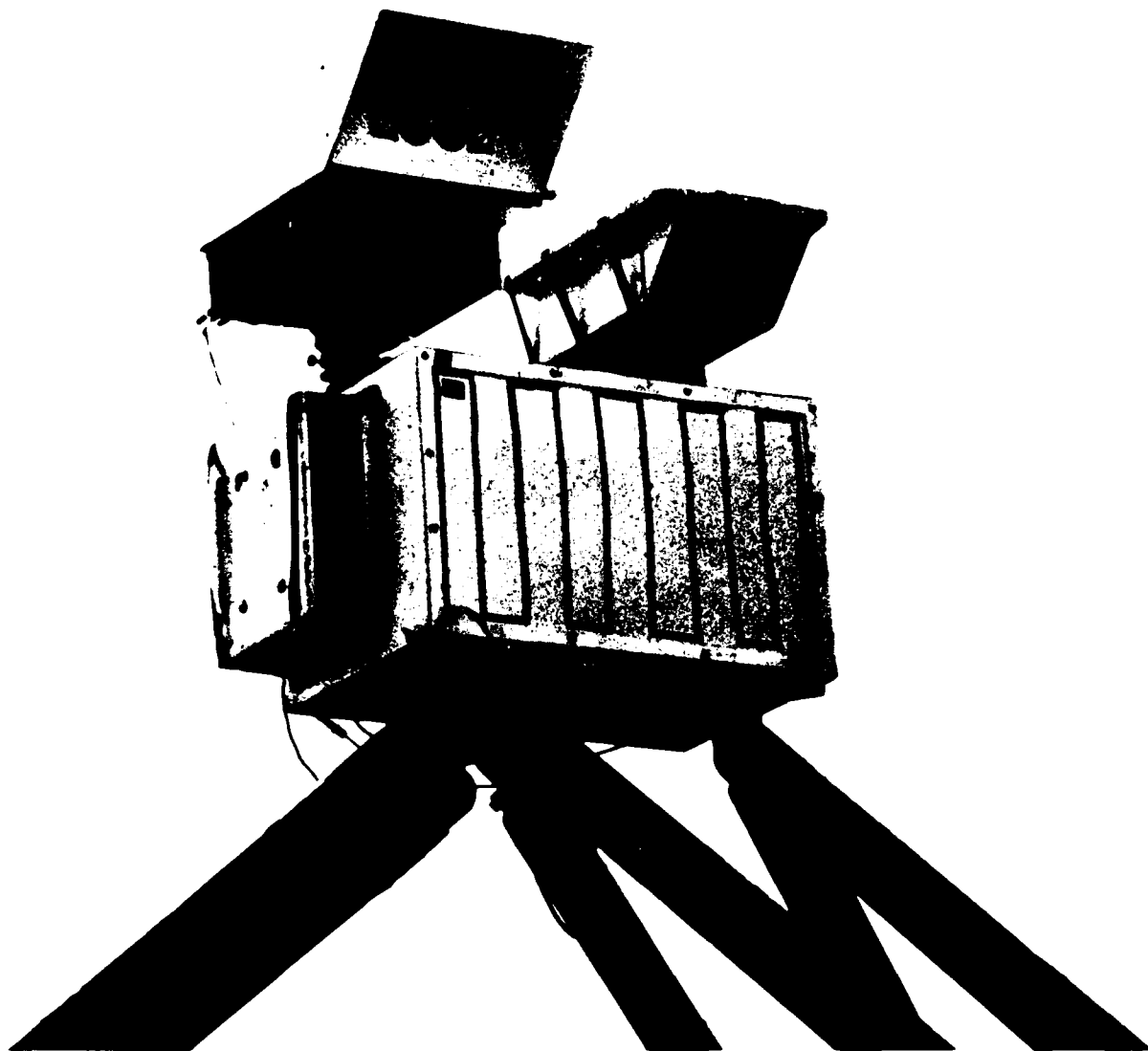
7

Figure 1.--Scintillation detectors. The lower box is the HCN receiver; it contains two 25-cm f/1 parabolic mirrors. The smaller box, mounted to the left of the lower box, contains the electronics. On top of the HCN receiver are the CO_2 receiver (left) and the LED receiver (right).
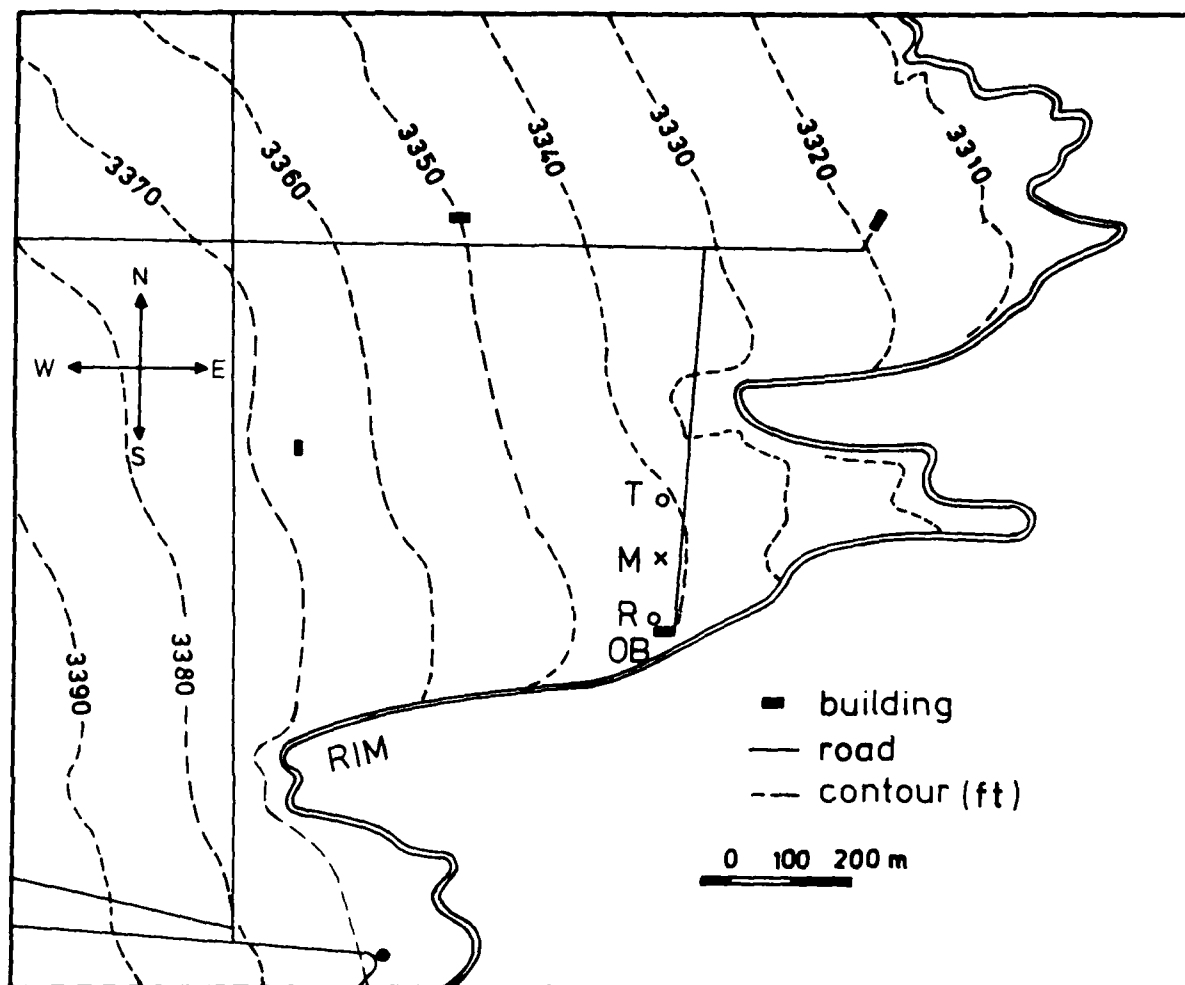
Figure 2.—Section of Table Mountain, indicating the positions of the transmitters (T), receivers (R), the masts with the in situ instruments (M) and the optical building (OB) where the signals were processed.

9

Furthermore, it is necessary to add a correction factor that accounts for the contribution of eddies near the inner scale of the turbulence, because the refractive-index spectrum exhibits a bump at the corresponding spatial wave numbers (Hill, 1978a). Taking these factors into account, the expressions for the scintillation are these:

0.94 μm: $\quad \sigma^2 = 1.54 \times 10^{10} \, C_n^{\,2} \, (0.809 + 0.920 \, \ell_o - 0.161 \, \ell_o^{\,2} - 0.177 \, \ell_o^{\,3})$

$$(0.4 \text{ cm} \lesssim \ell_o \lesssim 1.1 \text{ cm}) \qquad\qquad (9)$$

10.7 μm: $\quad \sigma^2 = 2.830 \times 10^{10} \, C_n^{\,2} \, (0.824 + 1.279 \, \ell_o - 0.736 \, \ell_o^{\,2})$

$$(0.3 \text{ cm} \lesssim \ell_o \lesssim 1.1 \text{ cm}) \qquad\qquad (10)$$

337 μm: $\quad \sigma^2 = 5.380 \times 10^{8} \, C_n^{\,2} \, (1.011 - 0.054 \, \ell_o + 0.088 \, \ell_o^{\,2})$

$$(\ell_o \lesssim 1.1 \text{ cm}) \qquad\qquad (11)$$

where

$$\sigma^2 = \frac{<(I_A - I_B)^2>}{<I>^2} \, . \qquad\qquad (12)$$

Here $C_n^{\,2}$ is in units $m^{-2/3}$; ℓ_o is the inner scale of turbulence in centimeters; $\ell_o = 7.4 \, \eta$, where η is the Kolmogorov microscale. (See, e.g., Hill and Clifford, 1978.) I_A and I_B are the light intensities observed in circular apertures labeled A and B. It is assumed that $<I_A> = <I_B> = <I>$. The apertures of the CO_2 and HCN transmitters are assumed to be infinitesimally small (point sources); the LED transmitter aperture-averaging effect must be taken into account. Transmitter and receiver aperture-averaging calculations give Eq. (9) for the LED scintillometer. Receiver aperture averaging calculations give Eqs. (10) and (11) for the CO_2 and HCN scintillometers. The calculations were done by R.J. Hill (private communication). The expression between parentheses is the inner-scale correction. It is small for the HCN scintillometer (2% at $\ell_o = 0.75$ cm), but quite considerable for the other two instruments (33% for the LED, and 37% for the CO_2 scintillometer at $\ell_o = 0.75$ cm). The inner-scale correction was calculated using the spectrum-with-bump for temperature only. This might not be accurate enough for the CO_2 scintillometer, where the correction is large and the differences between the
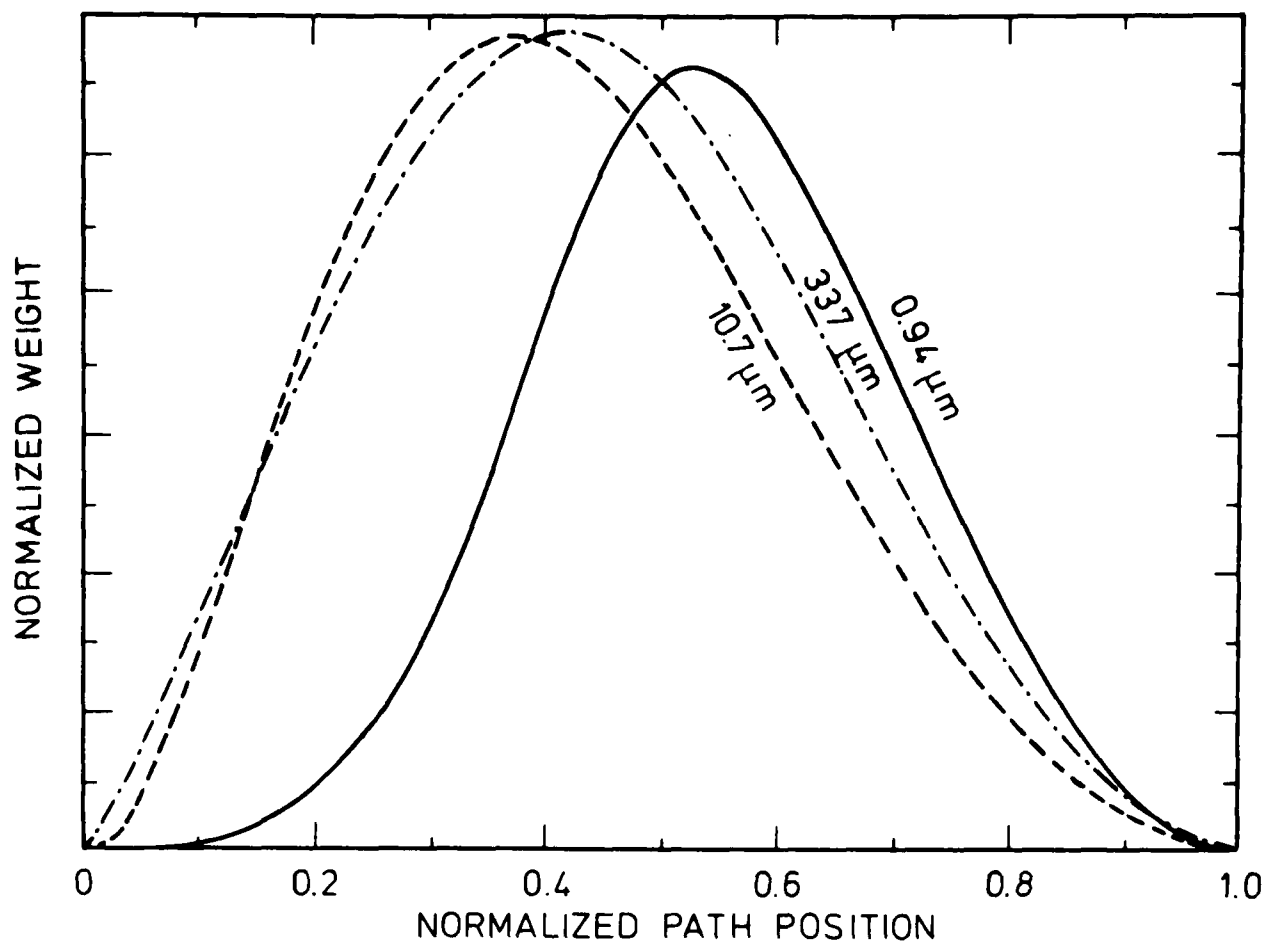
10

Figure 3.--C_n^2 path-weighting functions. The 0.94-μm curve is for a 5-cm tangent aperture receiver, 5-cm transmitter scintillometer. The inner scale is 0.75 cm for all cases. From R.J. Hill (unpublished).

temperature, humidity, and temperature-humidity spectra may be of importance. Caution has to be used if the third term in Eq. (6) is negative and tends to cancel the first two terms. The path-weighting functions for ℓ_o = 0.75 cm are shown in Fig. 3 (also calculated by R.J. Hill). Their shapes are not very sensitive to ℓ_o.

To illustrate the kind of signal we expect, σ^2 has been calculated for the case of C_T^2 = 0.367 K^2 $m^{-2/3}$, C_Q^2 = 0.367 x 10^{-6} kg^2 m^{-6} $m^{-2/3}$, C_{TQ} = $[C_T^2 C_Q^2]^{1/2}$, $<T>$ = 298 K and $<Q>$ = 10^{-2} kg m^{-3}. The results are shown in Table 3, where the scintillation signals $<(I_A - I_B)^2>^{1/2}$ are also given. These signals should be compared with the noise power. Noise power was derived from the manufacturer's data on the detectors, assuming a bandwidth of 100 Hz for the CO_2 and HCN detectors.

11

Table 3.—Expected performance of the scintillometers, based on Tables 1 and 2, and on formulas (9)-(11) with $\ell_o = 0.8$ cm.

$\lambda(\mu m)$	Power on detector (W)	$\dfrac{\langle(I_A-I_B)^2\rangle}{\langle I^2\rangle}$	$\langle(I_A-I_B)^2\rangle^{1/2}$ $= S$ (W)	Noise detector=N (W)	S/N	C_n^2 x inner scale corr. $(m^{-2/3})$
0.94	3.1×10^{-5}	74×10^{-3}	8.5×10^{-6}	--	*	3.95×10^{-13}
10.7	1.8×10^{-3}	11.1×10^{-3}	2.0×10^{-5}	3×10^{-8}	667	3.93×10^{-13}
337	2.4×10^{-5}	8.4×10^{-3}	2.2×10^{-7}	4×10^{-8}	5.5	1.57×10^{-11}

* The noise equivalent C_n^2 of the 0.94 μm LED scintillometer is lower than 10^{-16} $m^{-2/3}$.

It is seen that the HCN scintillometer has the lowest signal-to-noise ratio. The state of affairs represented in Table 3 is a rather optimistic one: C_Q^2 is very high in view of the often desiccated terrain of Table Mountain, and no account has been taken of other sources of noise, such as electronic and acoustic noise.

2.2 The 0.94-μm LED Scintillometer

For optical and mechanical details of the instrument the reader is referred to a report by Ochs et al. (1980). The transmitter was mounted on top of the trailer in which the CO_2 and HCN laser were located. The receiver was put on top of the HCN receiver box. Although initially a scintillometer with 15-cm apertures was used, it was replaced by one having 5-cm apertures, after some preliminary measurements. The reason was that the observed C_n^2 was several times larger than calculated from C_T^2 measurements with fast temperature sensors, and there was little experience with that scintillometer. But also the 5-cm aperture scintillometer gave too high a reading. It was next found that the effective aperture of the receivers was 4 cm rather than 5 cm, and that the transmitter aperture was partially coherent. The first effect accounts for an over-estimate of C_n^2 by a factor of $(5/4)^{7/6} = 1.24$; the second effect made the reading 1.62 times too high. (This was found by inserting a ground glass in front of the LED.) A third correction because of the receiver aperture separation of 6.7 cm

12

(center to center) is included in Eq. (9). The reading of the scintillometer was corrected for these effects and the comparison with the in situ observed C_n^2 is shown in Fig. 4. The correspondence at low wind speed is quite satisfactory, but at higher wind speeds (4 m s^{-1} has been used as the criterion) the optically observed C_n^2 is too high. Most likely, this is caused by vibrations of the detector box at higher wind speeds.

2.3 The 10.7-μm CO_2 Scintillometer

A Sylvania model 950 CO_2 laser served as radiation source. The laser was tuned to the P-30 line (10.697 μm) and had a continuous-wave output power of 5 W. Part of the light beam was reflected by a ZnSe plate to a thermopile radiation detector for monitoring the output power of the laser. Then the beam was compressed by means of two germanium lenses to one third of its original diameter, thus increasing the beam divergence by a factor of 3 to about 10 mrad and making the aiming of the beam at the receiver less critical. After passing an attenuator and a 260-Hz mechanical chopper, the beam was reflected upwards, led through an aluminum tube through the roof of the trailer, and directed to the receiver by means of a second mirror mounted on an adjustable support. Both mirrors were aluminum, front-surface plane mirrors. The distance from the beam compressor to the second mirror, as measured along the light path, was 2 m.

The receiver for the 10.7-μm scintillometer was mounted on top of the receiver for the 337-μm scintillometer, next to the 0.94-μm receiver. The two tangent circular apertures each have a diameter of 5 cm (which is nearly equal to the Fresnel zone size), and were covered with 10-μm-thick plastic foil to prevent air currents from entering the box. It was found that air currents seriously degrade the performance of the detector cells. The radiation was focused by two spherical mirrors (f = 28 cm) onto two pyroelectric detectors (Molectron P1-72) having a circular sensitive area of 2 mm diameter. The detectors were protected by germanium windows with an anti-reflection coating. The output signal of each detector was converted to a low impedance by a unity-gain amplifier mounted near the detector, and was then led through a two-stage amplifier (maximum gain 10,000 x) and a band-pass filter (gain 1.8 x, 3-dB points at 150 and 400 Hz), which were situated in a box mounted directly under the box containing the mirrors and detectors. The final
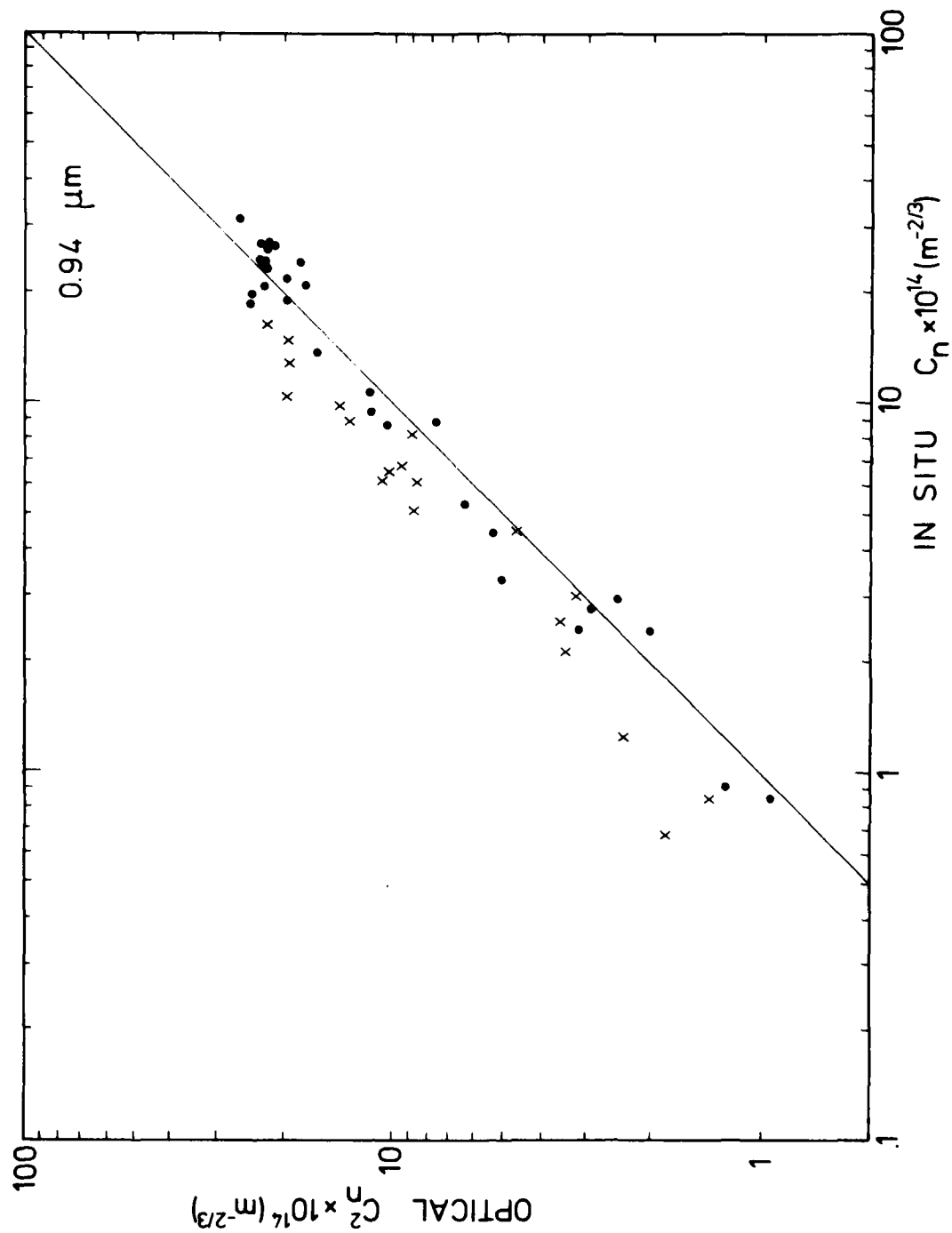
Figure 4.--C_n^2 from the 0.94-μm LED scintillometer, compared with C_n^2 calculated from C_T^2 measurements. The dots are for windspeeds lower than 4 m s^{-1}, the crosses for higher windspeeds.

14

output signal was maintained at a constant rms value by means of an automatic gain control feedback loop having a time constant of about 1 s. A schematic of the electronics is given in Appendix I. The electronic filters were chosen so that the amplitude-modulated 260-Hz carrier wave would pass freely, while other signals contributing only to the noise of the system were suppressed. The scintillation signal is expected to have dominant contributions from aperture-sized eddies, which are convected across the scintillation path by the wind. Thus, at a wind speed of 5 m s^{-1}, the frequencies of the scintillation are centered around 5 m s^{-1}/5 cm = 100 Hz.

The two output signals were processed by a Nova computer inside the building. During 16 minutes, 600 samples of each signal were taken, say A and B. Then the following quantity was calculated:

$$ S = \frac{< (\,|A| \; - \; |B| \; \frac{<|A|>}{<|B|>})^2 >}{<A^2>} \; . \tag{13}$$

By this procedure, the signals were demodulated and corrected for any difference in mean value (by the factor $<|A|>/<|B|>$). The angle brackets indicate the averages of the 600 samples. S is the same quantity as σ^2 in Eq. (12). This procedure was followed instead of an analog computation (as was done with the 0.95-μm scintillometer), because the analog demodulation of the signal offered problems caused by the large ratio of bandwidth to carrier frequency.

The computer has a time lag of 40 μs between the sampling of two neighboring channels. This was compensated by an approximately equivalent phase shift applied to one of the input signals, by means of an RC filter. The desired phase shift was $\phi = - 40 \times 10^{-6} \, \omega$ while that provided by the RC filter (RC = 40 × 10^{-6} sec) was $\phi = $ Arctan $(- 40 \times 10^{-6} \, \omega)$. The largest ω desired is very small compared to $(40 \times 10^{-6})^{-1}$ rad/sec; thus the two phase shifts are nearly equal because the arctangent is approximately linear in its argument provided the argument is much smaller than unity. The proper functioning of the procedure was checked with modulated sine-wave signals from sine-wave generators. With no modulation at all, the value of S was $\approx 2 \times 10^5$, a value thought to be caused by the 10-mV noise of the a-d converter. The noise level of S was sufficiently low compared with the expected signal level ($\sim 10^{-3}$).
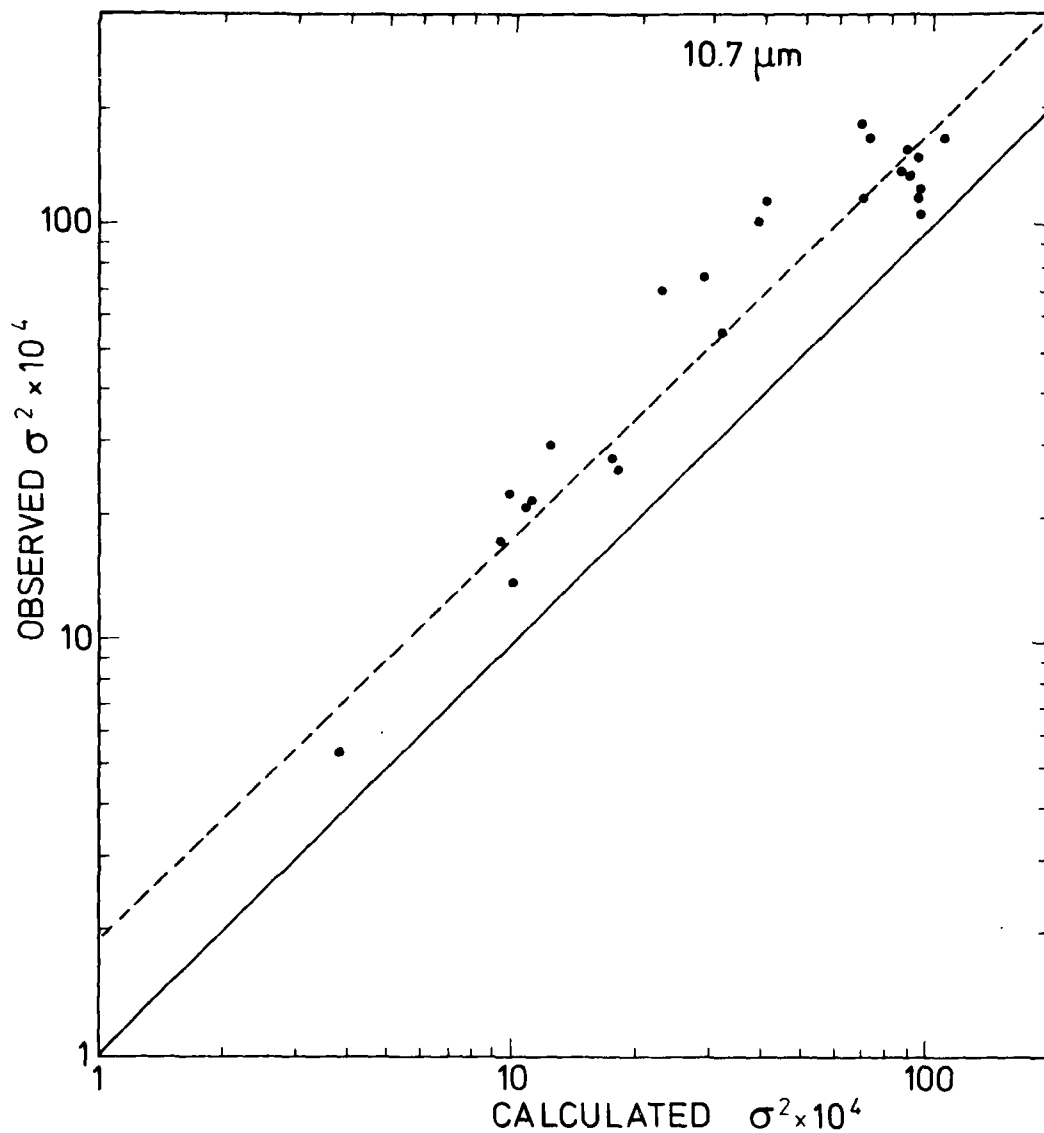
Figure 5.—Observed $\sigma^2 [=<(I_A-I_B)^2>/<I>^2)]$ of the 10.7-μm CO_2 scintillometer, compared with the same quantity calculated from measurements of C_T^2, C_Q^2, and C_{TQ}.

Measurements of σ^2 (= S) were compared with values calculated from in situ measurements of C_T^2, C_Q^2, and C_{TQ}, using fast temperature and humidity sensors. The contribution of C_Q^2 to C_n^2 was negligible, and that of C_{TQ} at most 20%. The results are shown in Fig. 5. It is found that the observed values of σ^2 are larger than the calculated values by a factor 1.5-2. Part of this discrepancy may be ascribed to instability of the pyroelectric detectors. It was noticed that the amplitude of the received signal showed, from time to time, irregular changes that were occasioned by neither the transmitter nor the atmosphere. The

16

changes were much faster than the response time of the automatic gain control loop. It is thought that a thermal imbalance between the detector cell and its environment might be responsible for this behavior, but time was lacking to investigate this problem. As a result, few conclusions can be drawn from the measurements with the CO_2 scintillometer.

2.4 The 337-μm Far-Infrared Scintillometer

The HCN laser that was used as a radiation source has a 4-m-long cavity with a folded confocal geometry (one flat mirror, and one concave mirror with a focal length of 8 m). As an output coupler, a polyethylene beam splitter arranged in a Michelson interferometer configuration was used. Output coupling could thereby be varied between 0% and 16%. Details of the laser can be found in a report by Wells et al. (1971). Because of the cavity geometry, the output beam should have a diameter of 4.1 cm close to the laser and finally reach a full-angle divergence of 10 mrad.

The laser was powered by a regulated 3000-V d.c. power supply with a ballast resistor of 1 kΩ in series. At a discharge current between 0.7 and 1 A, the anode-cathode voltage is ∿2000 V. A constant flow of 20 cm^3/min (STP) of a mixture of He, N_2, and CH_4 (in the ratio 3:36:8) is maintained through the Pyrex discharge tube. The lasing HCN gas is produced by chemical reactions in the discharge. A constant gas pressure in the tube is rather easily produced by equilibrium between the gas supply rate (provided by a gas cylinder filled with the proper mixture, and a fine needle valve) and the pumping rate (provided by a mechanical vacuum pump).

The composition of the gas fed to the laser was chosen on the basis of a publication of Belland and Véron (1973), who claimed that when this mixture was used the discharge tube remained clear, in contrast to the brown deposit that usually forms on the wall, and the output power was high. While our discharge tube stayed clean, the output power was less than expected on the basis of calculations and experiments of Belland et al. (1976). This may be attributed to the non-optimum tube diameter (8 cm), and non-optimum electrode geometries. The highest output power, obtained at a gas pressure of 1.2 torr, was ∿50 mW. The discharge was then rather turbulent, however. At even higher gas pressures the

17

power supply could not meet the higher voltage demand of the discharge; consequently, the current dropped, and so the lasing power. At lower gas pressures the discharge became less turbulent, until at $\sim$0.9 torr a stable, striated discharge was obtained with $\sim$30 mW in the 337 μm line. (Line identification was simple with the Michelson interferometer output coupler.) After a considerable warming-up period ($\sim$1 hour) the laser usually ran very stably.

An effort was made to get a stable discharge with a higher laser power. Other gas mixtures were tried (our mix with CH_4 or NH_3 added, and a mix of CH_4 and NH_3 only), the gasflow, discharge current, and gas pressure were varied, and other electrode geometries were used, but all with little or no improvement.

An effort was made to measure the beam diameter and divergence. To do this, apertures were put in the beam at positions between 0.15 and 10.1 m from the exit window. Directly after the aperture, the radiation was focused by a polyethylene lens on a thermopile detector. In this way the beam diameter was sensed. It was observed that the beam diameter at the exit window was $\sim$2 cm, instead of the 4 cm calculated, and that the beam divergence was about the expected value, 10 mrad. However, about a 50% radiation loss was observed at 10.1 m, which cannot be explained by divergence nor by absorption.

The laser beam was chopped at 150 Hz, led through an aluminum tube through the roof of the trailer and aimed at the receiver in much the same way as for the CO_2 laser beam. A plastic beam splitter reflected part of the beam onto a Teflon lens, which focused the radiation on a pyroelectric detector that served as a monitor. The distance from the laser exit window to the mirror on top of the trailer was 3.35 m.

The receiver unit was a box containing two 25-cm-diameter tangent mirrors and two pyroelectric detectors. The mirrors had a focal length of 25 cm, and were machined from cast aluminum to a parabolic shape by the NBS mechanical workshop. The pyroelectric detectors (Molectron P1-73) had a sensitive circular area of 3 mm diameter and Teflon windows (0.8 mm in thickness). The radiation entered the detector box through another Teflon window, 1.5 mm thick. By these windows, an effective blocking of the CO_2 radiation was achieved: the transmission at 10.7 μm

18

was estimated at 10^{-6}; at 337 μm it was 0.7. The area of the pyroelectric detectors was large enough to accommodate for mirror imperfections (the image of a point source is blurred, and has a diameter of ~1 mm), and for a possible tilt of the wavefront at the receiver (which might let the focal spot wander over at most 1 mm).

Signal processing was along the same lines as for the CO_2 scintillometer. The signals were first amplified (gain 2x) near the detectors, then led to a small box mounted to the box containing the mirrors and detectors, where a maximum gain of 2.5×10^4 was applied; finally the signals passed a bandpass filter (3-dB points at 80 and 240 Hz). The total maximum gain was 1.7×10^5, and the final output signals were maintained to a constant root-mean-square value by means of an automatic gain control. The expected maximum bandwidth of the signal was 40 Hz. In order to suppress 60-Hz pickup, the electronics were powered by batteries placed inside the box. The electrical schematic is given in Appendix I.

In operating the HCN scintillometer, it was found that the system was severely hampered by instability of one of the pyroelectric detectors. (The same problem was found with the CO_2 scintillometer, but to a lesser extent.) Most of the time, no measurement could be made at all. On only one day did the system operate reasonably well for a couple of hours. A value of 7×10^{-4} was observed for σ^2; the calculated value was 8×10^{-6}. Obviously, only the noise of the system at that particular moment of time was observed. The low calculated value of σ^2 indicates the kind of problem one faces in trying to observe scintillation with submillimeter waves in a very dry atmosphere: it is often too low to be detectable. During a period of three months (January through March 1981) on only one day (2 February) were the humidity fluctuations strong enough to give an observable $\sigma^2 = 1.2 \times 10^{-3}$. Unfortunately, on that day the scintillometer did not work.

It is suggested that before making new attempts to observe scintillation at 337 μm, one should first have a thorough look at the functioning of pyroelectric detectors in a poorly temperature-controlled environment. If the use of such a detector is too marginal, other devices should be considered, like a germanium bolometer, though these detectors have to be cooled to cryogenic temperatures, which offers some technical complications.

3. IN SITU MEASUREMENTS--THE INSTRUMENTS

These micrometeorological in situ measurements were acquired to serve as a reference for the optical measurements, and to give additional meteorological information:

(a) Wind speed and wind direction with a Gill propeller vane.

(b) Air temperature and dewpoint temperature with an EG&G model 220 system.

(c) Net radiation with a Swissteco radiometer.

(d) Temperature fluctuation, and temperature difference, using three 2-μm-diameter Pt wires.

(e) Humidity fluctuations, using two Ly-α hygrometers.

(f) Vertical wind speed fluctuations, with a 20-cm-path sonic anemometer.

An example of the arrangement of the sensors (a), (d), (e), and (f) is given in Fig. 6. These sensors were mounted at a height of 4 m on top of two well-guyed poles situated at the midpoint of the optical path. The sensors were located so that the following quantities could be measured:

(a) $C_T{}^2$, from the temperature difference of two Pt sensors.

(b) $C_Q{}^2$, from the humidity difference of two Ly-α hygrometers.

(c) C_{TQ}, from one pair of temperature sensors and one pair of humidity sensors.

(d) Sensible heat flux, by correlating the vertical wind speed with the temperature fluctuation measurement.

(e) Latent heat flux (or moisture flux), by correlating the vertical wind speed with humidity fluctuations.

The orientation of the separation between the two Ly-α hygrometers was manually set to near perpendicularity to the wind direction. That means that cross-wind structure parameters were observed. There is evidence that there is no difference between crosswind- and streamwise-measured structure parameters (Wyngaard et al.,

20

1978). No experimental evidence is available regarding vertically measured struc-
ture parameters.

The distance between the Pt wires and the center of the Ly-ι humidiometers
was set at 3.7 cm. The wires were positioned upwind from the Ly-ι's. It is
assumed that the presence of the Ly-α's does not significantly disturb the advected
temperature field. Some support of this assumption was found by observing the
temperature variance at various distances between a temperature sensor and a Ly-ι.
Another Pt wire was at a fixed position and served as a reference. Over the
whole range of available distances, 10.5 to 2.5 cm, no difference was noted. In
another experiment, two temperature spectra were measured sequentially, one with
the sensor at 4 cm from the Ly-ι axis, the other with the sensor on the axis, and
thus in the gap between the source and detector. The spectra were similar.

The distance between the axis of the sonic anemometer and the temperature
and humidity sensor to be correlated with vertical wind was 10 cm at most.

The propeller vane was situated close to the turbulence instruments because
the windspeed is needed for subsequent data analysis, where Taylor's hypothesis
is used for the calculation of structure parameters from time-lagged measurements
(see Section 4). The other instruments--the net radiometer and the temperature/
dewpoint instrument--were situated at some distance from the poles. The tempera-
ture, dewpoint temperature, and net radiation measurements served for obtaining
general meteorological information. The dewpoint temperature measurements were
further used for calibrating the Ly-α humidiometers, as is discussed below. All
instruments were set up permanently in the field, with the exception of the Ly-ι
hygrometers and the Pt temperature sensors. The signals were amplified close to
the instruments before being transported to the Nova computer inside the building
(the only exception being the signal of the net radiometer, which was directly
connected to the building). There, a final amplification was performed to ac-
commodate the signal level to the $\pm$ 5-V input range of the computer. Special care
had to be taken to avoid ground loops between the computer ground and the instru-
ments.

Next, we shall pay some special attention to the Ly-ι hygrometer. The reason
for using the Ly-ι line (121.6 nm) for measuring humidity is that the ratio of

22

water vapor and oxygen absorption shows a remarkable peak very close to the Ly-α line (Tillman, 1965). Furthermore, the absorption is fairly strong, thus making measuring over a short path (∿1 cm) possible. Another important consideration is that the construction of a Ly-α source, a hydrogen discharge tube, is relatively easy. A nitric oxide ionization chamber is usually used as a detector. Both source and detector should have special windows for transmitting the Ly-α radiation. The best choice seems to be magnesium fluoride, which resists the weather (especially moisture-resistant) fairly well. Magnesium fluoride is opaque below 115 nm, while the ionization potential of nitric oxide is at 135 nm. The detector is thereby sensitive to the wavelength interval 115-135 nm only, which nicely brackets the Ly-α line (121.6 nm). Since no other means of spectral filtering can be used in the field, it is important to have the emission of the Ly-α line as pure as possible in order to minimize the absorption by spurious oxygen lines. Spectral purity can be controlled by the choice of gas mixture and pressure in the discharge tube. An important refinement is the addition of a UH_3 reservoir to the discharge tube. Uranium hydride provides a constant, low, hydrogen pressure if heated. In this way a very pure Ly-α source with a lifetime of more than 1000 hours is obtained (Buck, 1977). A disadvantage of the UH_3 source might be its larger size in comparison with the "conventional", unheated source, which makes it more likely to obstruct the airflow through the gap between source and detector. However, little is known about this effect. We preferred to use the conventional tube.

The manner in which the sources and detectors were mounted is shown in Fig. 7. A small box, containing two amplifiers, was situated about 0.5 m from the detectors. (For the electronic schematic, see Appendix II.) The output voltage was about 1 V. The frequency response of the amplifiers was d.c. to 500 Hz (3-dB point). A laboratory test, where the frequency response of the Ly-α hygrometer was measured by electronic modulation of the source current, showed that these amplifiers essentially limited the over-all response of the hygrometer. With faster amplifiers, an almost flat frequency response from d.c. to 10 kHz was found (J.T. Priestley and W.D. Cartwright). The output voltage fluctuations (reflecting humidity fluctuations) we observed were often so small that it was necessary to offset the output voltage and amplify it again in order to boost the fluctuating signal sufficiently above the computer noise (∿10 mV). The noise of the hygrometer, as measured at the output of the first amplifier, was less than 1 mV peak-to-
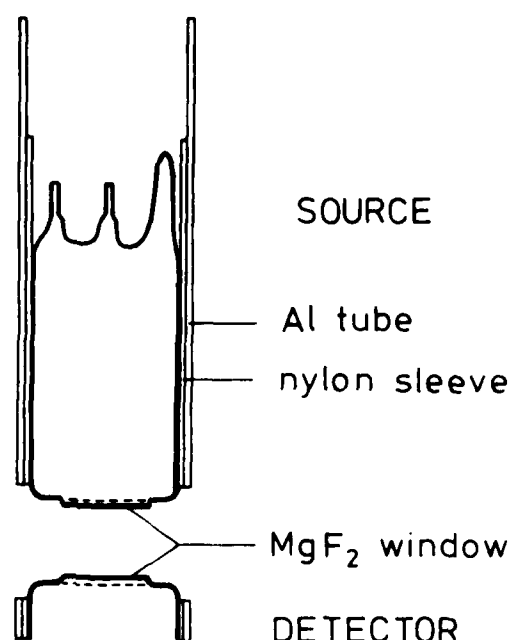
SOURCE

— Al tube

— nylon sleeve   Figure 7.--Construction of a Ly-α
                   hygrometer.

— MgF$_2$ window

DETECTOR

peak, which corresponds to a humidity noise of 0.01 g m^{-3} or less. The offset of
the amplifiers can easily be checked by blocking the light path. It should be less
than 1 mV. We found that it had to be adjusted only very rarely.

The humidity was calculated from the output voltage of the hygrometers, using
a procedure of Buck (1980). The procedure is based on laboratory calibrations of
similar sources and detectors, and accounts for additional oxygen absorption.
Also, a correction factor for the changing collimation with different distances
between source and detector is included. The calculation, which was performed on
the Nova computer, also involved a calibration "constant". This constant was
obtained by comparison with an absolute hygrometer, in our case the dewpoint in-
strument. It was necessary to adjust this calibration constant frequently because
drift of the Ly-α hygrometers could be as high as 10% per hour. To do so, each
computer sample of the two Ly-α hygrometers was compared with the reading of the
dewpoint hygrometer, and the constant was adjusted slightly (fractional change 5 x
10^{-5}). By this procedure a drift rate of 10% per hour could be compensated, with-
out affecting the fluctuations.

The limited experience we have gained with the Ly-α hygrometer as an outdoor
instrument is not positive in all respects. Although the instrument should be

24

rugged enough to withstand all kinds of weather, it was found that the lifetime of the detectors was less than the several hundred hours anticipated. Detector failure was, in all cases, occasioned by leaks in the sealing between the magnesium fluoride window and the Pyrex tube. In one case, the detectors failed after an exposure of several weeks to varying weather, including freezing rain and snow, with only 20 hours of operation. The failure was manifested by an initially low detector resistance, followed by a high resistance but low sensitivity. After this experience, it was decided to put the instrument outside only during measurements. Since then, the hygrometers have performed more satisfactorily.

4. DATA PROCESSING AND ON-LINE CALCULATIONS

Data processing was done on a Nova computer. The computer had no facility for storing data on disc or magnetic tape. Therefore, the calculation of mean values, variances, structure functions, etc., had to be done on-line. A disadvantage of this system is that it is not possible to calculate spectra. For a few runs, however, we recorded data of the fast temperature sensor and one Ly-α hygrometer on an analog tape recorder and digitized these data later. An advantage of the on-line calculations is that there is an immediate check on sensor performance.

The computer was run with either of two programs: a program called METEO, handling nine input channels with a sampling rate of 142 Hz, and a program called SCINT, handling fourteen channels at 50 Hz. The sampling rates are for both cases the highest possible. The reason for having a high sampling rate will be made clear below. The input channels for METEO are the two Ly-α hygrometers, fast temperature, fast temperature difference, sonic anemometer, net radiation, wind speed, temperature, and humidity. SCINT handles the same inputs, plus one channel for the 0.94 μm scintillometer, and two channels for each of the other two scintillometers.

The high sampling rate was for calculating structure parameters from time-lagged observations. For instance, the observation of the humidity Q at time

points t_o and $t_o + \tau$ enables one to calculate the humidity structure parameter by $<[Q(t_o) - Q(t_o + \tau)]^2>(<u>\tau)^{-2/3}$, where $<u>$ is the mean windspeed for the period of observation considered. The shortest possible time delay τ is obviously set by the sampling rate of the computer. The purpose of these measurements is to investigate the supposed independence between structure parameters and distance r by simply varying the time delay. The alternative method, an array of many sensors, is less attractive.

In more detail, the data processing is as follows. The computer takes in data during 1 second. Using program SCINT, the first sample of the 142 samples for each channel is stored, and only for the fast temperature channel and one Ly-α channel the samples 3, $3+2^i$ (i=0,1,2,...), up to 131 and 142 are retained. The latter samples serve for calculating time-lagged structure parameters. With program METEO, the samples 3, 4, 5, 7, 11, 19, 35, and 50 are stored for this purpose. The temperature and humidity differences are related to the third sample because it was found that at a sampling rate of 142 Hz the time interval between the first and the second sample was longer than 1/142 s, and the interval between the second and the third sample was too large at times. After all data are transferred into physical quantities, a number of calculations are performed (like squaring, cross products, etc.), and the results are stored. This takes about 0.5 second. Then, the next 1-second block of data is taken in. After a run of 600 blocks, which takes about 16 minutes, mean values are calculated and printed on a teletype.

Next, we give formulas that were used for the calculation of variances, structure parameters, etc. Time averaging is denoted by angle brackets.

The variance of a quantity x, $v(x)$, is calculated with

$$v(x) = <x^2> - <x>^2 . \tag{14}$$

Variances were calculated for the horizontal wind speed (u), the vertical wind speed (w), fast temperature (T_A), and one Ly-α sensor (Q_A).

The skewness of temperature and humidity was calculated by

$$S(x) = \frac{\langle x^3 \rangle - \langle x \rangle^3}{[v(x)]^{3/2}} \; . \tag{15}$$

Structure parameters were calculated as follows:

$$c^2_{Qr} = [\langle (Q_A - Q_B)^2 \rangle - \langle Q_A - Q_B \rangle^2)/r^{2/3} \; , \tag{16}$$

$$c^2_{Q\tau} = \langle [Q_A(t_o) - Q_A(t_o + \tau)]^2 \rangle / (\langle u \rangle \tau)^{2/3} \; , \tag{17}$$

$$c^2_{Tr} = \langle (\Delta T)^2 \rangle / r^{2/3} \; , \tag{18}$$

$$c^2_{T\tau} = \langle [T_A(t_o) - T_A(t_o + \tau)]^2 \rangle / (\langle u \rangle \tau)^{2/3} \; , \tag{19}$$

$$C_{TQr} = \langle (\Delta T)(Q_A - Q_B) \rangle / r^{2/3} \; , \tag{20}$$

$$C_{TQ\tau} = \langle [T_A(t_o) - T_A(t_o + \tau)] \; x$$

$$[Q_A(t_o) - Q_A(t_o + \tau)] \rangle / (\langle u \rangle \tau)^{2/3} \; . \tag{21}$$

Structure parameters calculated from sensors separated by a distance r are denoted by the subscript r; those calculated with time delay are marked with subscript τ. In formula (16) the mean difference between the two Ly-α hygrometers has to be included, because generally $\langle Q_A \rangle \neq \langle Q_B \rangle$. The temperature difference signal ΔT is filtered by a 1/60-Hz high-pass RC filter, which guarantees that $\langle T_A - T_B \rangle = 0$.

The vertical fluxes of heat (Q_o) and water vapor (E_o) are calculated by

$$Q_o = \langle wT_A \rangle - \langle w \rangle \langle T_A \rangle \tag{22}$$

and
$$E_o = \langle wQ_A \rangle - \langle w \rangle \langle Q_A \rangle \; . \tag{23}$$

The average of the vertical wind, $\langle w \rangle$, is included since it is not necessarily zero. Apart from an instrumental offset, $\langle w \rangle$ will differ from zero because of the expansion of air while heated (or compression if cooled). Moreover, the sonic anemometer has been aligned with the vertical, and is thus not perpendicular

to the slightly sloping (1 degree) terrain. This may result in an offset in the vertical wind, because the mean wind follows the terrain and may have a vertical component.

The correlation coefficient r_{TQ} of temperature and humidity was calculated by

$$r_{TQ} = \frac{<T_A Q_A> - <T_A><Q_A>}{[v(T_A)\ v(Q_A)]^{1/2}} \quad . \tag{24}$$

The σ^2 of the 10.7 and of the 337-μm scintillometers was calculated according to equation (13). The output signal of the 0.94-μm scintillometer had only to be averaged.

5. RESULTS OF THE IN SITU MEASUREMENTS

5.1 The Temperature Structure Parameter and Spectrum

In Section 4 two methods for measuring C_T^2 are mentioned: the time-lagging method, using one sensor, and the method with two spaced sensors. In Fig. 8 the results of the two methods are compared by plotting the quantity $C_{T\tau}^2/C_{Tr}^2$ as a function of $<u>\tau$, which is the product of the mean windspeed and the time delay. This product is equivalent to a spatial spacing. The fixed distance between the two sensors for measuring C_{Tr}^2 was 0.31 m. In both examples the data points scatter around the line $C_{T\tau}^2/C_{Tr}^2 = 1$ up to $<u>\tau \sim 1$ m, where $C_{T\tau}^2$ drops below C_{Tr}^2. Probably, at $<u>\tau > 1$ m outer-scale effects enter, which means that the contributing eddies are larger than inertial subrange eddies. In this report, the structure function multiplied by spacing to the -2/3 power, i.e., $D(<u>\tau)[<u>\tau]^{-2/3}$ is loosely referred to as the structure parameter; strictly speaking, this quantity is equal to the structure parameter only when the spacing, e.g., $<u>\tau$, is in the inertial subrange of spatial sizes.

The measurements at small $<u>\tau$ (the lowest value observed is $\sim 10^{-2}$ m) may be contaminated by noise. It was observed that the noise of the temperature-measuring equipment was equivalent to a $(0.03°C)^2$ variance of the time-lagged temperature difference, resulting in a noise value of $0.2°C^2$ m$^{-2/3}$ for $C_{T\tau}^2$ at

28

$<u>\tau = 10^{-2}$ m. The observed values of C_{TT}^2 at that spacing were of the order of $0.1°C^2 \ m^{-2/3}$, so a noise contribution of 20% is likely. An increase of that magnitude may indeed be recognized in the January example in Fig. 8. In Fig. 9 the theoretical dependence of the structure parameter on r/ℓ_o is shown in the case of the Hill spectrum. A decrease of $D_T(r)/r^{2/3}$ is anticipated at $r/\ell_o < 2$. Putting $\ell_o = 0.6 \times 10^{-2}$ m (a value appropriate to the left-hand data points in Fig. 8), one arrives at the conclusion that $D_T(r)/r^{2/3}$ should be nearly constant down to $r \sim 1.2 \times 10^{-2}$ m. The observations seem to be in accordance with this conclusion.

The proportionality of $D_T(r)$ with $r^{2/3}$ is a direct consequence of the shape of the temperature spectrum in the inertial subrange. The structure function $D_T(r)$ and the one-dimensional spectrum $F_T(\kappa)$ are related by the expressions

and

$$D_T(r) = 8\pi \int_0^\infty (1 - \frac{\sin \kappa r}{\kappa r}) \ \phi_T(\kappa)\kappa^2 \ d\kappa \qquad (25)$$

$$F_T(\kappa_1) = 4\pi \int_{\kappa_1}^\infty \phi_T(\kappa) \ \kappa \ d\kappa \ , \qquad (26)$$

where $\phi_T(\kappa)$ is the spatial spectrum. These relations are valid only if the turbulence is isotropic. In the inertial-convective range (Corrsin, 1951)

$$\phi_T(\kappa) = (4\pi \ \kappa^2)^{-1} \ \beta \ \chi \ \varepsilon^{-1/3} \ \kappa^{-5/3} \ , \qquad (27)$$

where χ is the rate of dissipation of temperature variance, ε the rate of dissipation of turbulent kinetic energy, and β a constant ($\beta = 0.72$ according to Hill, 1978b). Combining Eqs. (25)-(27) gives

$$D_T(r) = (9/10) \ \Gamma(1/3) \ \beta \ \chi_T \ \varepsilon^{-1/3} \ r^{2/3} \ , \qquad (28)$$

which demonstrates that $D_T(r)/r^{2/3}$ is independent of r. Let us now suppose that $\phi_T(\kappa) \sim \kappa^{p-2}$. It is easily found that
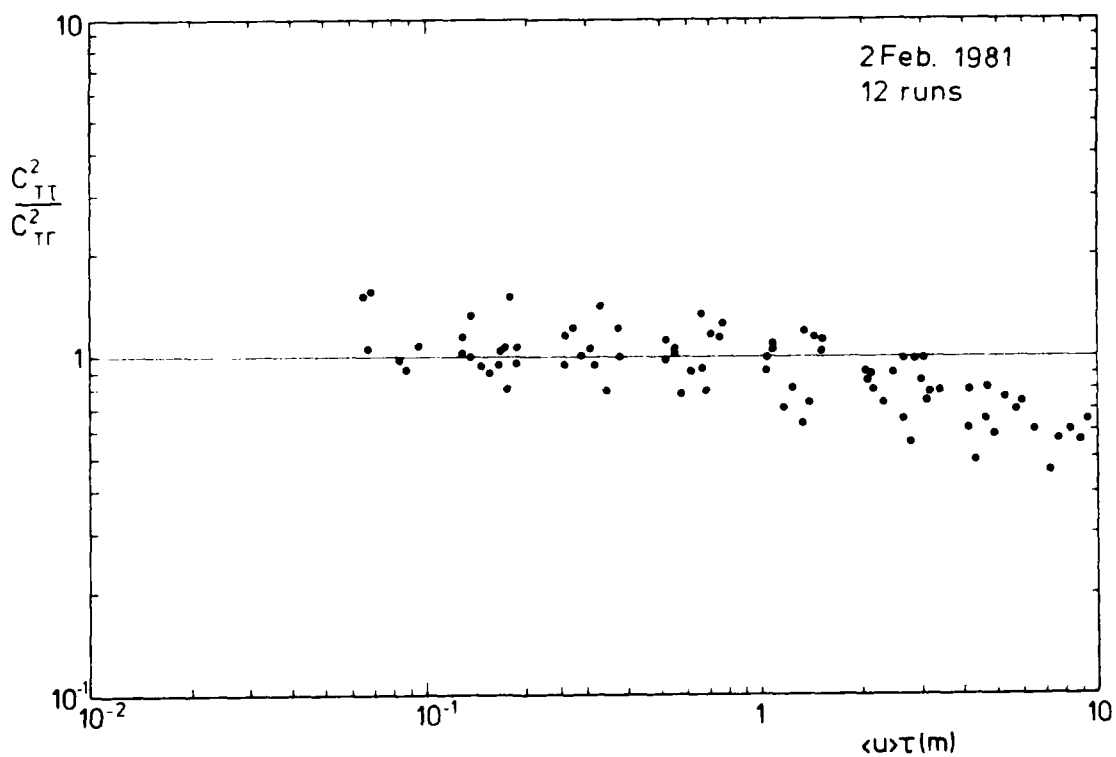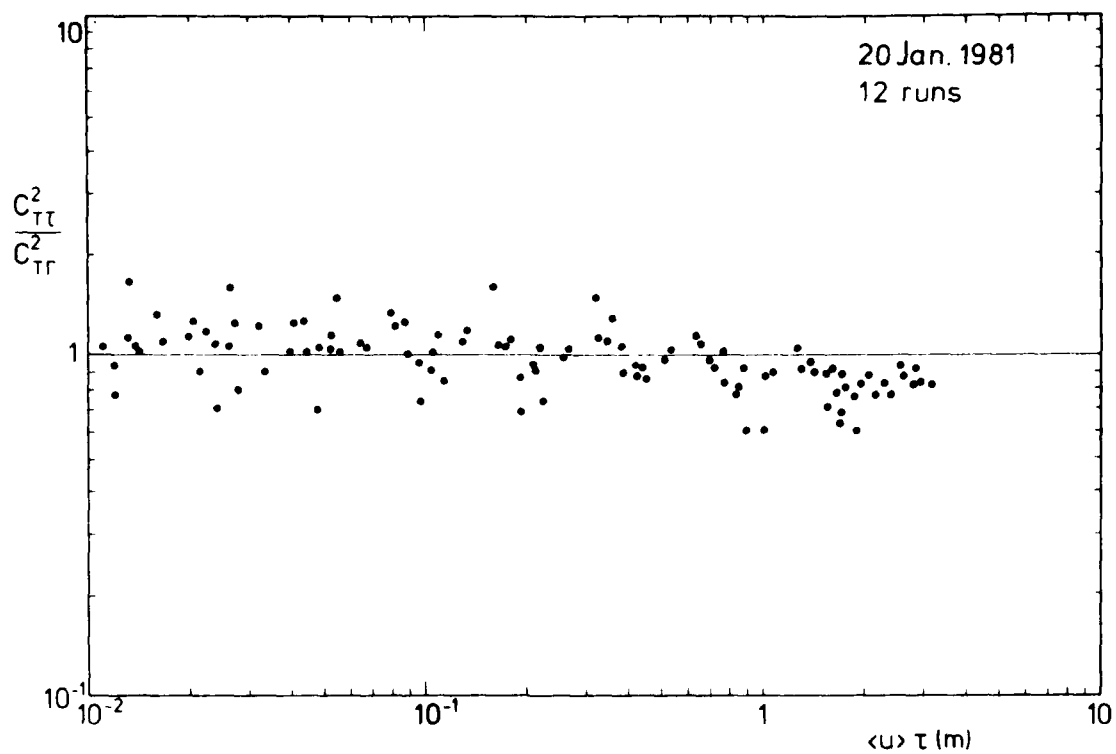
Figure 8.--Two examples of time-lagged observations of the temperature structure parameter $(C_{T\tau}^2)$, divided by spaced-sensor observations of the same quantity (C_{Tr}^2), versus the time-lagged spacing $<u>\tau$. The spacing r was 0.31 m.
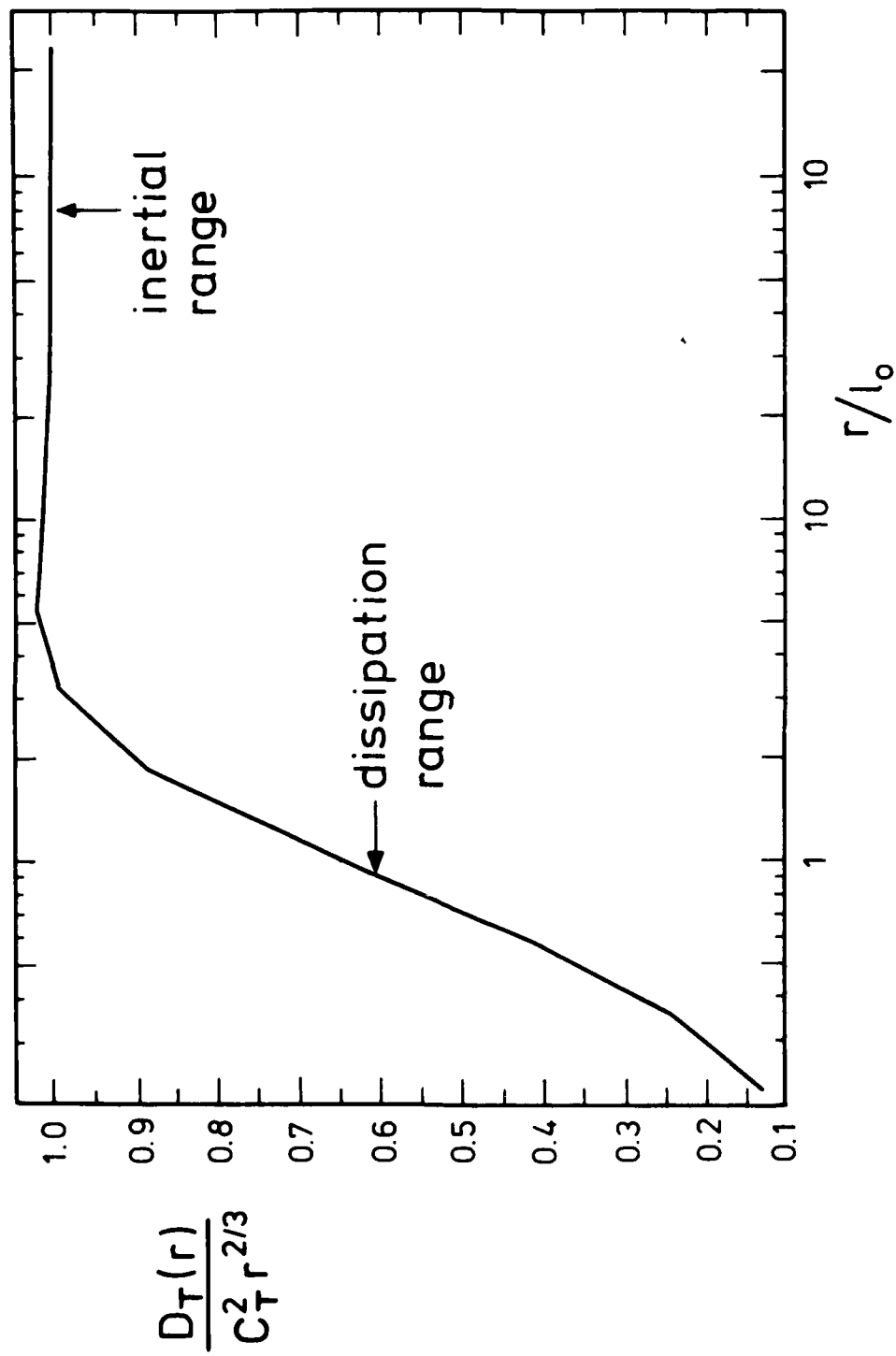
30

Figure 9.--The temperature structure function $D_T(r)$ divided by $r^{2/3}$, and normalized to the structure parameter C_T^2, versus r/ℓ_o, where ℓ_o is the inner scale. From R.J. Hill (unpublished).

31

$$D_T(r) \sim r^{-(p+1)} \int_0^\infty (1 - \frac{\sin y}{y}) y^p \, dy \quad . \tag{29}$$

The integral converges for $-3 < p < -1$. Then, $D_T(r) \sim r^{-(p+1)}$. The one-dimensional spectrum has the form

$$F_T(\kappa) \sim \chi_T \, \epsilon^{-1/3} \, \kappa^p \quad . \tag{30}$$

Relations (29) and (30) demonstrate the link between the wavenumber dependence of the spectrum, and the distance dependence of the structure function.

The inertial subrange behavior of the temperature spectrum was observed directly by spectral analysis of the temperature signal. During five runs, the signal was recorded on an analog tape recorder and digitized afterwards at 400 Hz. Before digitizing, the signal passed a low-pass filter with half-power point at 100 Hz and a negligible transmission at the Nyquist frequency (200 Hz). Each run of about 15 minutes was cut into sections of 10 seconds duration. An FFT procedure was applied to each section. Finally, the spectra of the sections were averaged to produce the spectrum for the whole run. A consequence of this procedure is that no information is obtained for frequencies lower than 0.1 Hz. One of the temperature spectra is shown in Fig. 10. In the dimensionless frequency interval $nz/\langle u \rangle \sim 1$ to 50 the spectrum follows the $n^{-5/3}$ inertial subrange prediction. At frequencies higher than 50 the cutoff of the electronic filter becomes noticeable.

5.2 The Humidity Structure Parameter and Spectrum

Results of the time-lagged and spaced-sensors techniques for measuring the humidity structure parameter are shown in Fig. 11. As with the temperature case, the spacing between the two sensors was 0.31 m. For the February data in Fig. 11, it is seen that the observed values of $C_{Q\tau}^2/C_{Qr}^2$ scatter around unity for $\langle u \rangle \tau$ between 10^{-1} m and 2 m, but the January data lie $\sim 15\%$ above unity. The difference between the two month's data can hardly be explained by instrumental effects (like the effect of $\langle Q_A \rangle \neq \langle Q_B \rangle$, which will be discussed later). Possibly a anisotropic behavior of the atmosphere is involved, resulting in larger values
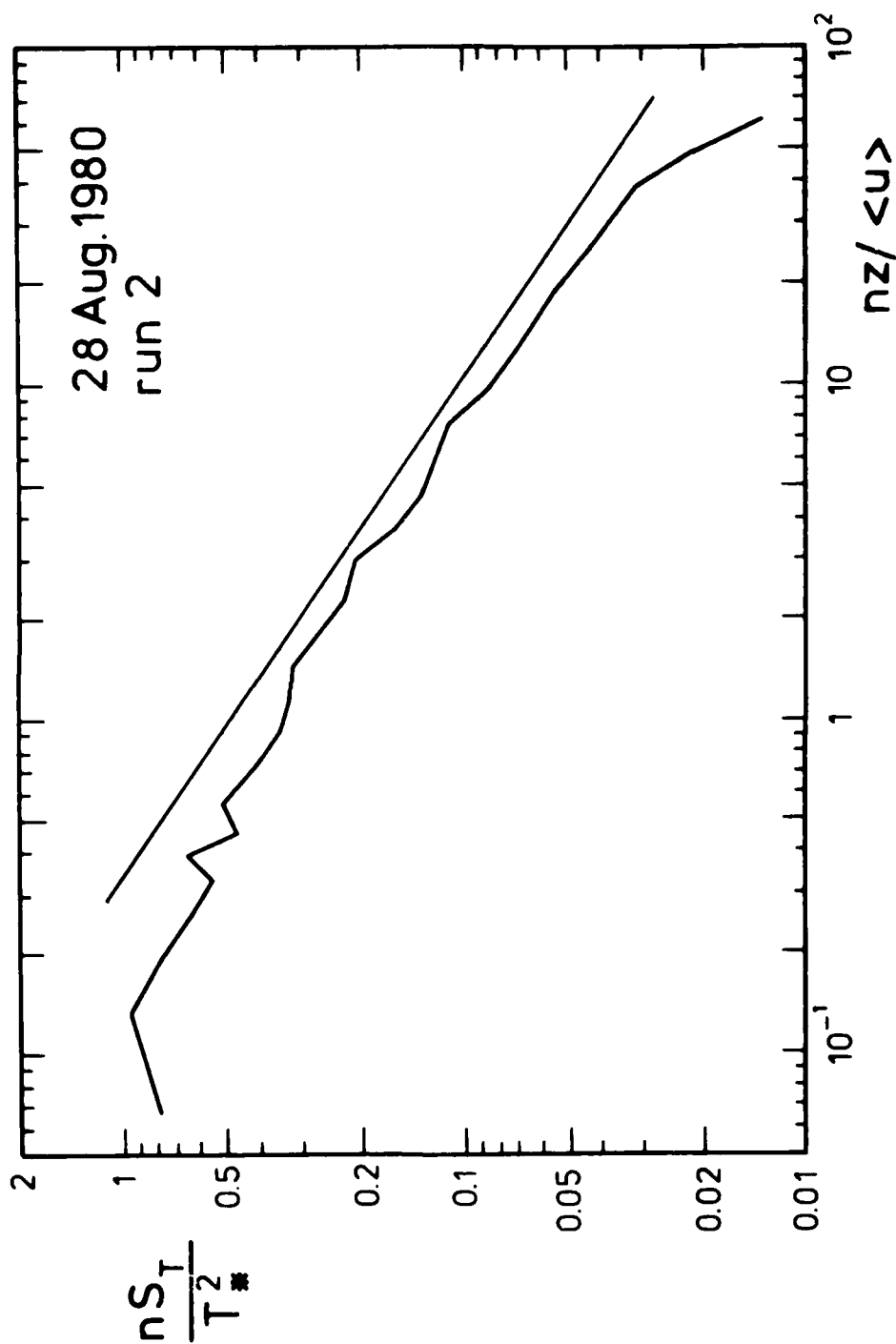
32

Figure 10.—The normalized temperature spectrum. T_* was calculated by $\langle w'T'\rangle/u_*$; the calculation of u_* is discussed in Section 5.4. The straight line corresponds to a $n^{-5/3}$ dependency of the spectrum.
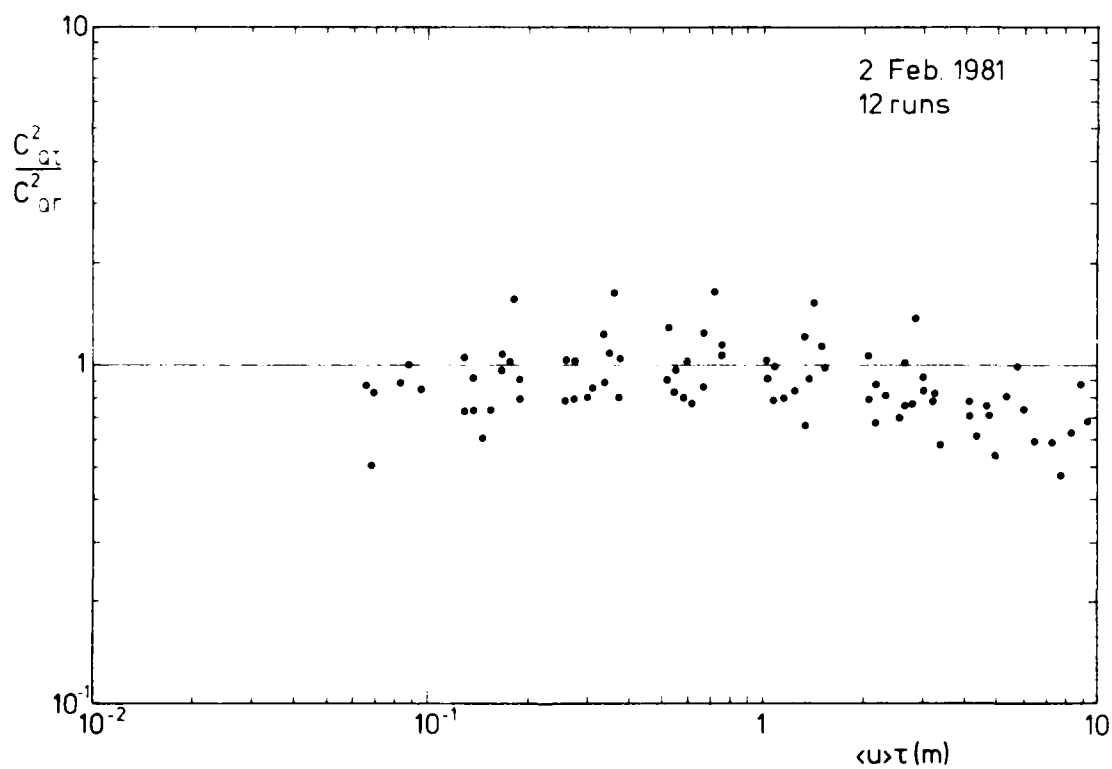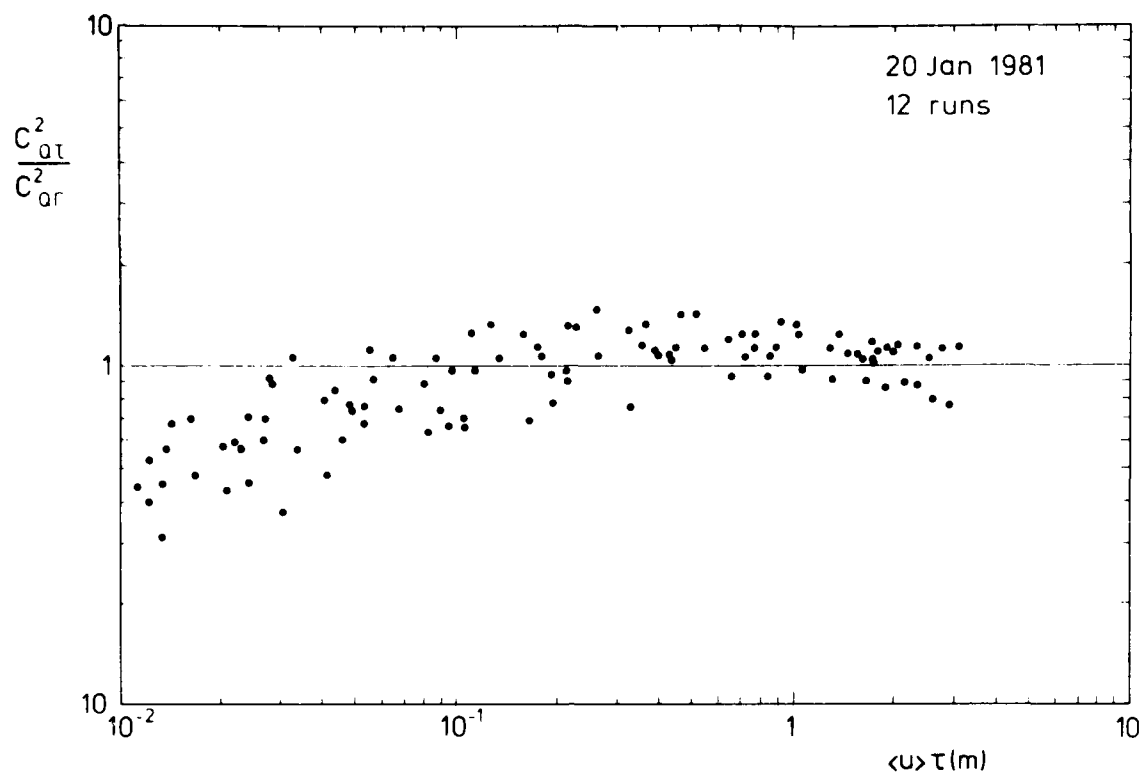
33

Figure 11.--Two examples of time-lagged observations of the humidity structure parameter divided by spaced-sensor observations of the same quantity, versus the time-lagged spacing.

of $C_Q{}^2$ if observed streamwise ($C_{Q\tau}^2$) than observed across-wind (C_{Qr}^2). The January

observations in Fig. 11 were done at a lower wind speed (1-3 m s^{-1}) than those

in February (3-9 m s^{-1}), so the anisotropic character could disappear with in-

creasing wind speed. Any anisotropy should also be evident when comparing

$C_{T\tau}^2/C_{Tr}^2$ for the two data sets in Fig. 8; however, no deviation from unity is

evident at inertial range spacings in Fig. 8. Another cause of $C_{Q\tau}^2 > C_{Qr}^2$ might

be failure of Taylor's hypothesis if the wind speed is not constant. The time-

lagged structure parameters have to be reduced by a correction that depends on

$\sigma(u)/<u>$. The corrections are the same as the ones calculated by Wyngaard and

Clifford (1977) for the spectra. In the present case, such corrections are only

a few percent at most.

For $<u>\tau > 2$ m, $C_{Q\tau}^2/C_{Qr}^2$ drops below unity, similar to the behavior of

$C_{T\tau}^2/C_{Tr}^2$. Also for $<u>\tau < 0.1$ m, $C_{Q\tau}^2/C_{Qr}^2$ is less than unity. This latter drop-off

at small spacings is probably due to the response characteristics of the Ly-α

hygrometer, which also affect the observed humidity spectra (Fig. 12). Starting

from dimensionless frequency $nz/<u> \gtrsim 0.5$, the spectrum follows the -5/3 power law,

up to $nz/<u> \sim 10$; from then on, the observed spectral density is too low. The

spectral density is about half its expected value at $n = 50$ Hz (observed from

five spectra). The cutoff is as if the Ly-α had a time constant of $\sim 3 \times 10^{-3}$ s.

Using this time constant and a mean wind speed of 4 m s^{-1}, an unpublished calculation

by Wyngaard shows that the observed value of C_{Qr}^2 is expected to be 70% of its true

value at a sensor spacing of $r \sim 6 \times 10^{-2}$ m. This compares rather well with the

observed spacing $<u>\tau \sim 4 \times 10^{-2}$ m for a 70% response.

The "effective" time constant of 3×10^{-3} s is larger than the response time

of the Ly-α as observed in the laboratory (i.e., 0.3×10^{-3} s, see Section 3).

The effect of space averaging should be small; according to calculations of Andreas

(1981) for a cylinder having a diameter of 0.8 cm and a length of 1 cm (values

appropriate to the Ly-α), the spectral density is only slightly under-estimated at

large $nz/<u>$ (see Fig. 12). Also, the effect of flow distortion was investigated.

For this purpose, we compared the spectra of the temperature and the humidity of a

measurement where the Pt-wire was inside the gap of the Ly-α hygrometer, with those

of successive measurement where the temperature sensor was at its usual position, 4

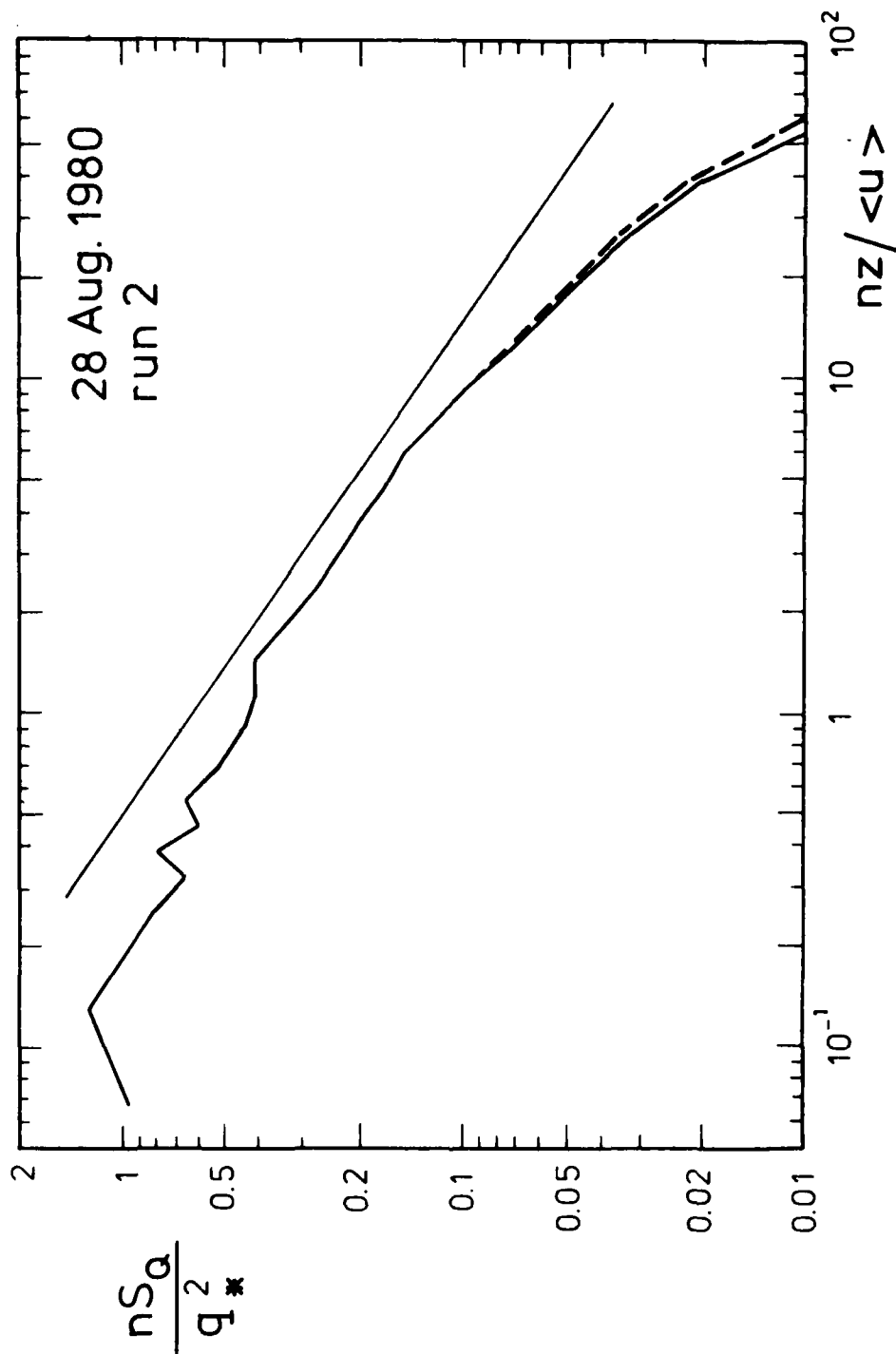cm upstream of the Ly-α. If there were an effect of flow distortion, it would

35

Figure 12.--The normalized humidity spectrum. The straight line corresponds to the -5/3 inertial sub-range power law; the broken line is the observed spectrum after having applied corrections for space averaging (Andreas, 1981).

hygrometer, with those of successive measurement where the temperature sensor was at its usual position, 4 cm upstream of the Ly-α. If there were an effect of flow distortion, it would likely be present in both the humidity spectrum and the temperature spectrum. Figure 13 shows that the temperature spectra of both situations are very much alike (as are the humidity spectra, Fig. 14), which indicates that there is no effect of flow distortion on the observed humidity spectra. Concluding, we cannot offer an explanation for the 3×10^{-3} s "effective" time constant of the Ly-α.

Some remarks have to be made on the stability of the Ly-α hygrometer relative to the measurement of structure parameters. In calculating C_{Qr}^2 (Eq. (16)) allowance has been made for $<Q_A> \neq <Q_B>$ by subtracting $<Q_A - Q_B>^2$ from $<(Q_A - Q_B)^2>$. However, this is not a full correction because sensor drift will also have an effect on the level of the fluctuations. An analysis (Appendix III) shows that considerable errors can be made in the calculation of C_{Qr}^2 if the average humidities differ by more than a few percent. So, it is necessary to adjust the calibration constants of the Ly-α's in such a way that $<Q_A>$ is very nearly equal to $<Q_B>$, before a series of runs starts. Once started, the drift correction procedure (see Section 3) will generally maintain $<Q_A> = <Q_B>$. Still, there remains a pitfall. The drift of a Ly-α may exceed the level of turbulent humidity fluctuations during a run (a run takes about 16 minutes). This happens if the humidity fluctuations are very low (say, less than 0.5% of the mean humidity) and the drift rate is normal ($\sim 2\%$ per hour), or if the drift rate is high (over 50% per hour was observed with a "dying" detector) and the humidity fluctuations are moderate. Then, while the drift correction procedure is still capable of keeping $<Q_A> = <Q_B>$ (if necessary, the drift correction procedure can be adjusted to cope with a high drift rate), it cannot suppress, and may even generate, slow fluctuations with amplitude equal to or less than that of the turbulent fluctuations. These slow, instrumental fluctuations may contribute considerably to C_{Qr}^2; in fact, an increase by a factor of 2 and more has been noted. This is a problem specific to the spaced-sensors method; the time-lagging method is insensitive to long-period fluctuations whatever the source may be. Hence, the time-lagging technique is preferred here over the spaced-sensors technique.

The noise of the Ly-α's is mostly not affecting the measuring of C_Q^2. Depending on the humidity, and the detector-source separation, the noise level is
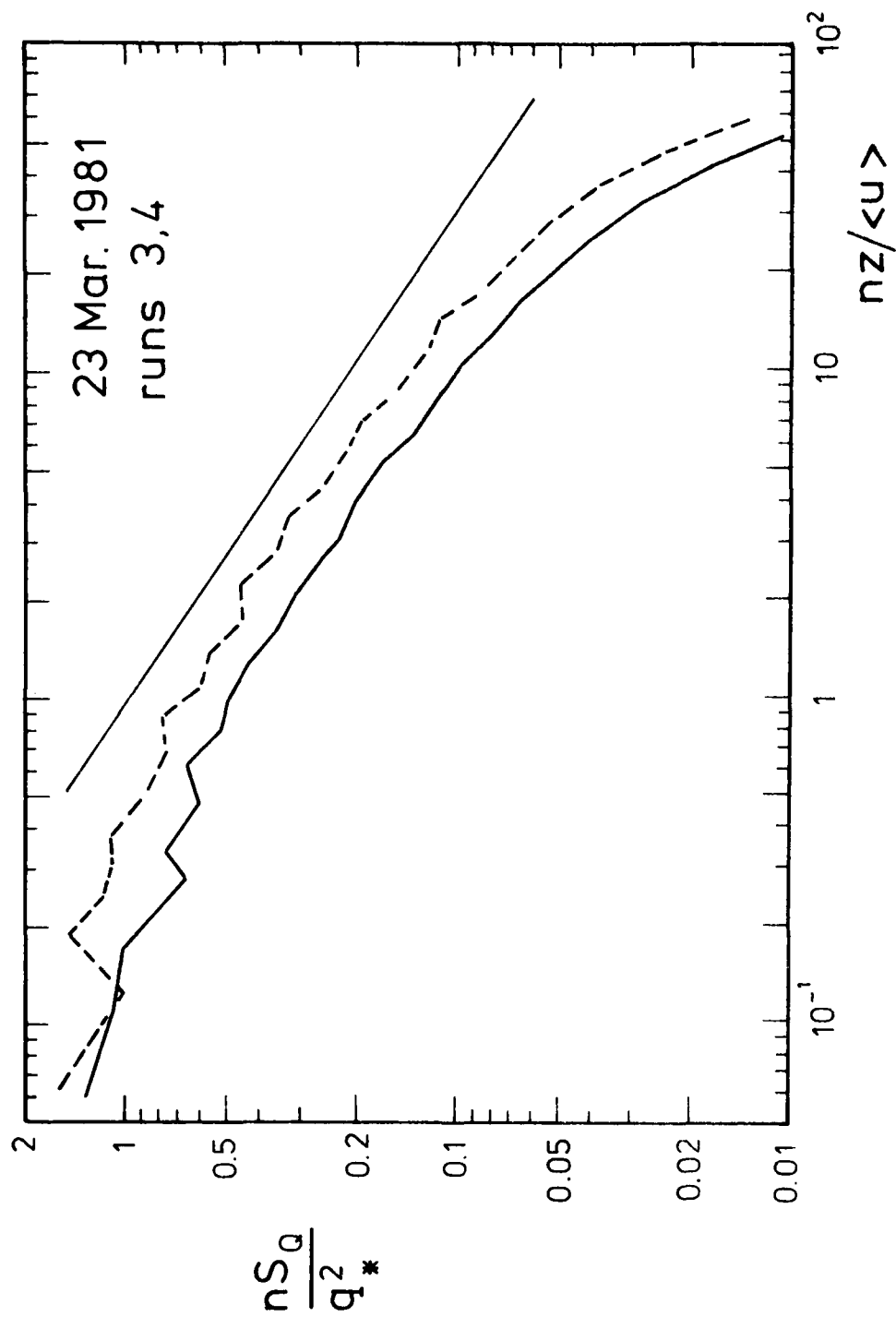
37

Figure 13.--Observations of the temperature spectrum with the temperature sensor in the center of the Ly-α gap (dashed curve), and 4 cm upwind from the gap (solid curve). The straight line indicates the -5/3 inertial subrange power law.
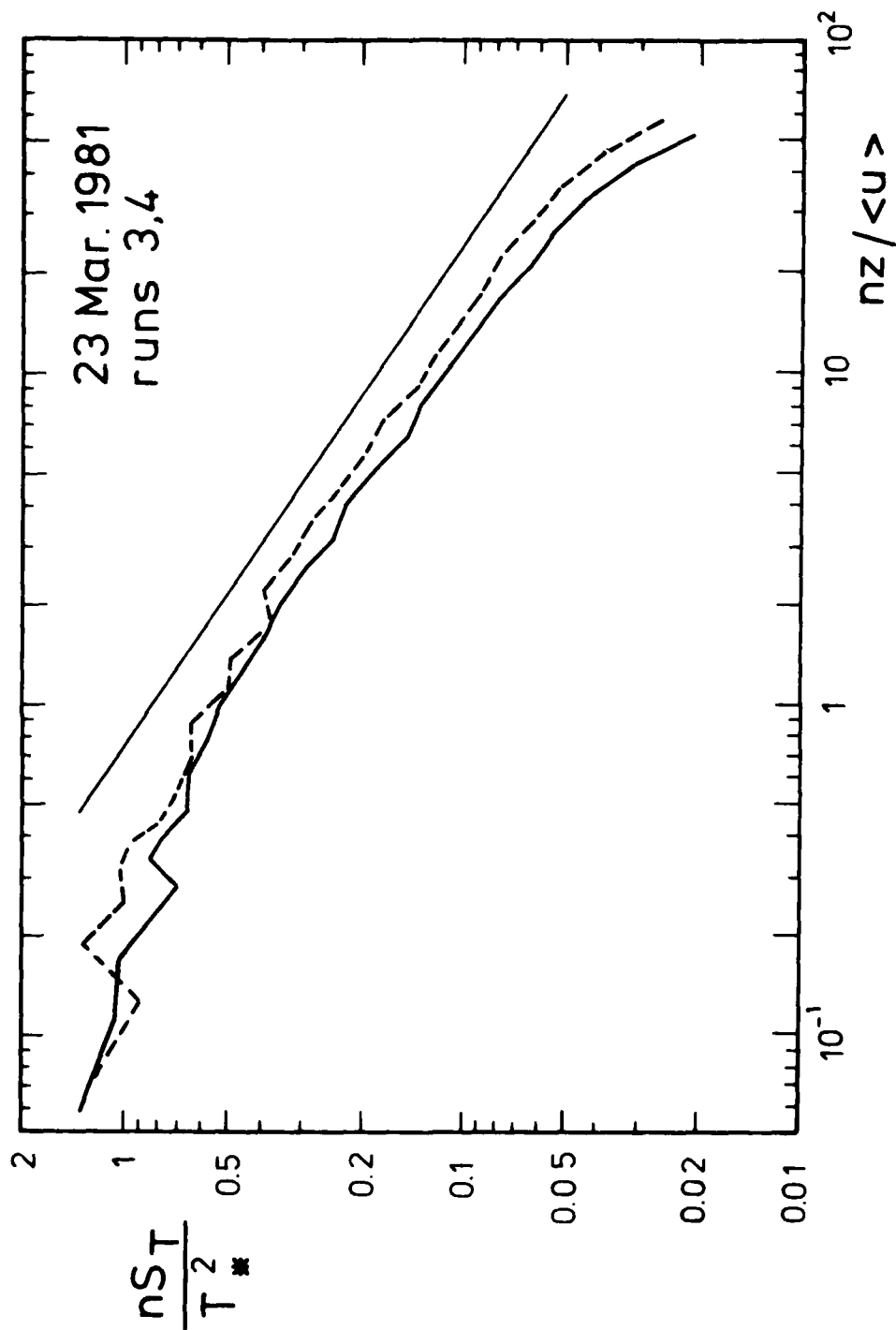
Figure 14.—Observations of the humidity spectrum with the temperature sensor in the center of the Ly-α gap (dashed curve), and 4 cm upwind from the gap (solid curve). The straight line indicate the -5/3 inertial subrange power law.

39

in the range of 10^{-3} to 10^{-2} g m^{-3} (peak-to-peak), which results in a noise contribution to C_Q^2 of 5×10^{-7} to 5×10^{-5} (g m$^{-3})^2$ m$^{-2/3}$ if the sensor separation is 0.31 m, and 5×10^{-6} to 5×10^{-4} (g m$^{-3})^2$ m$^{-2/3}$ at a separation of 0.01 m. Observed values of C_Q^2 are usually more than 10^{-3} (g m$^{-3})^2$ m$^{-2/3}$.

5.3 The Temperature-Humidity Structure Parameter and Spectrum

There are two striking aspects of the plots of $C_{TQ\tau}/C_{TQr}$ in Fig. 15: $C_{TQ\tau}/C_{TQr} \approx 1.2 - 1.4$ for $<u>\tau$ between 0.3 and 3 m, and there was an early fall-off of C_{TQ} at small values of $<u>\tau$. Regarding $C_{TQ\tau} > C_{TQr}$, only anisotropic behavior of the turbulence can be offered as an explanation; we cannot explain, however, why it should be more prominent in C_{TQ} than in C_Q^2, and is lacking in C_T^2.

The drop-off of $C_{TQ\tau}/C_{TQr}$ at $<u>\tau < 0.2$ m was likely caused by the joint effects of the finite distance between the temperature sensor and the humidity sensor, and the "effective" response time of the humidity sensor. Due to the latter effect, an extra "spacing" of the order of the mean wind speed times the response time might be introduced (for example, with $<u> = 4$ m s^{-1} and $\tau_{Ly-\alpha} = 3 \times 10^{-3}$ s, the extra spacing is 1.2 cm; the instrumental spacing was usually 4 cm). The two effects would act in the same direction because the temperature sensor was positioned upstream (and slightly to one side) of the humidity sensor. Consequently, one would expect that the drop-off occurs at higher values of $<u>\tau$ the higher the wind speed is. The wind speed was 3 to 9 m s^{-1} for the February data in Fig. 15, whereas it was 1 to 3 m s^{-1} for the January data, but no clear difference in the drop-offs of the two data sets can be seen (taking into account the slightly larger values of $C_{TQ\tau}/C_{TQr}$ of the January data at $<u>\tau \sim 1$ m). Also, the February data, if split into a high wind speed part and a low wind speed part, does not show the expected behavior. Some effect of the sensor spacing may be recognized in Fig. 16.

The temperature-humidity cospectrum was calculated for several runs. An example is shown in Fig. 17. We have to make a reservation here, as the cospectral density is much less (by roughly a factor of 10) than the cospectral density implied by the structure parameter. So, any conclusion drawn from our cospectra should be considered tentative. From Fig. 17 it is seen that an $n^{-5/3}$ line might
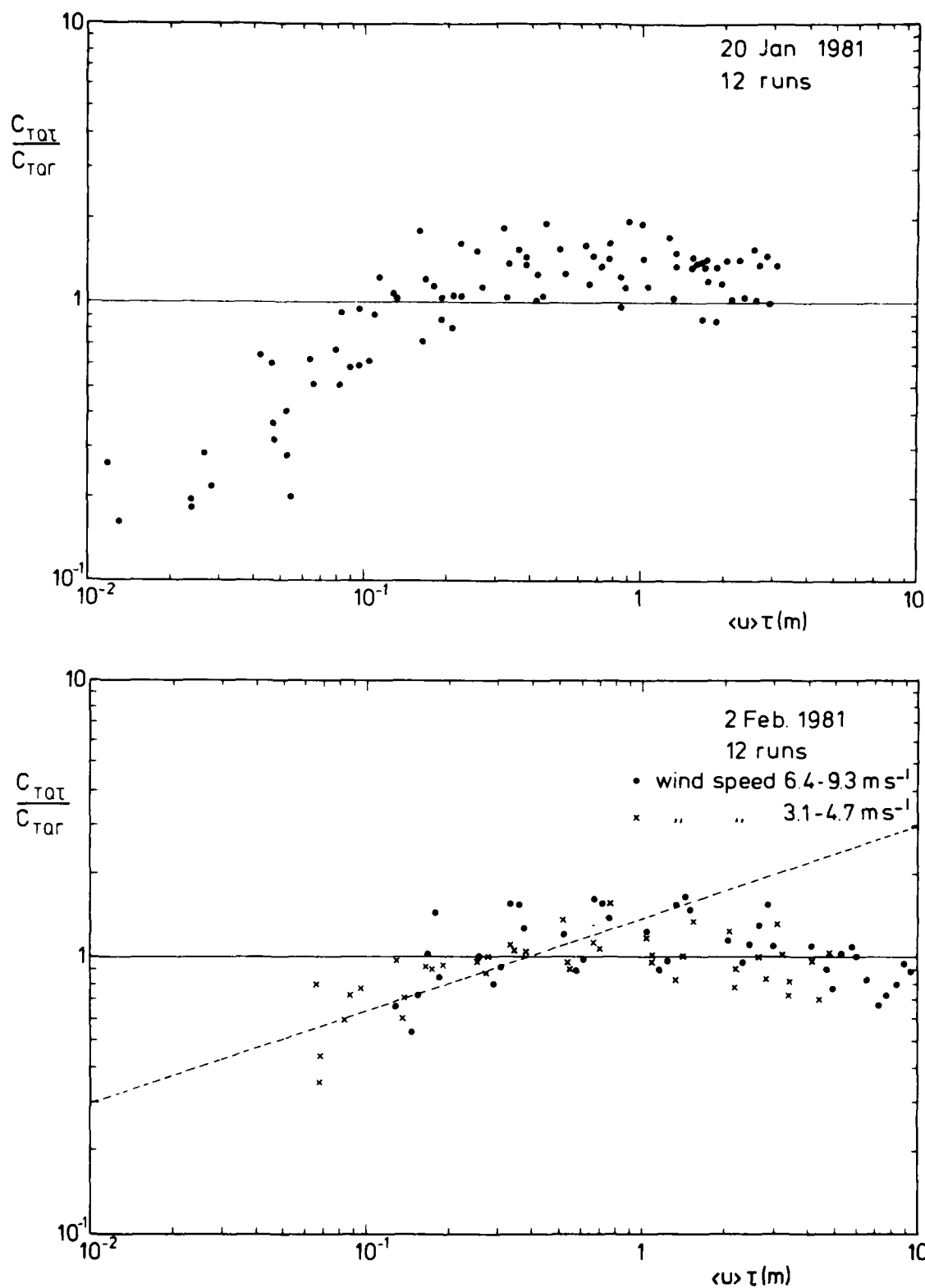
10

$\dfrac{C_{T\Omega\tau}}{C_{T\Omega r}}$

20 Jan 1981

12 runs

1

10^{-1}

10^{-2} 10^{-1} 1   10

⟨u⟩τ (m)

10

$\dfrac{C_{T\Omega\tau}}{C_{T\Omega r}}$

2 Feb. 1981

12 runs

• wind speed 6.4-9.3 m s⁻¹

× „   „   3.1-4.7 m s⁻¹

1

10^{-1}

10^{-2} 10^{-1} 1   10

⟨u⟩τ (m)

Figure 15.—Two examples of time-lagged observations of the temperature-humidity
structure parameter divided by spaced-sensor observations of the same quantity,
versus the time-lagged spacing. The dashed line in the second example cor-
responds to a n^{-2} dependency of the temperature-humidity cospectrum.

41
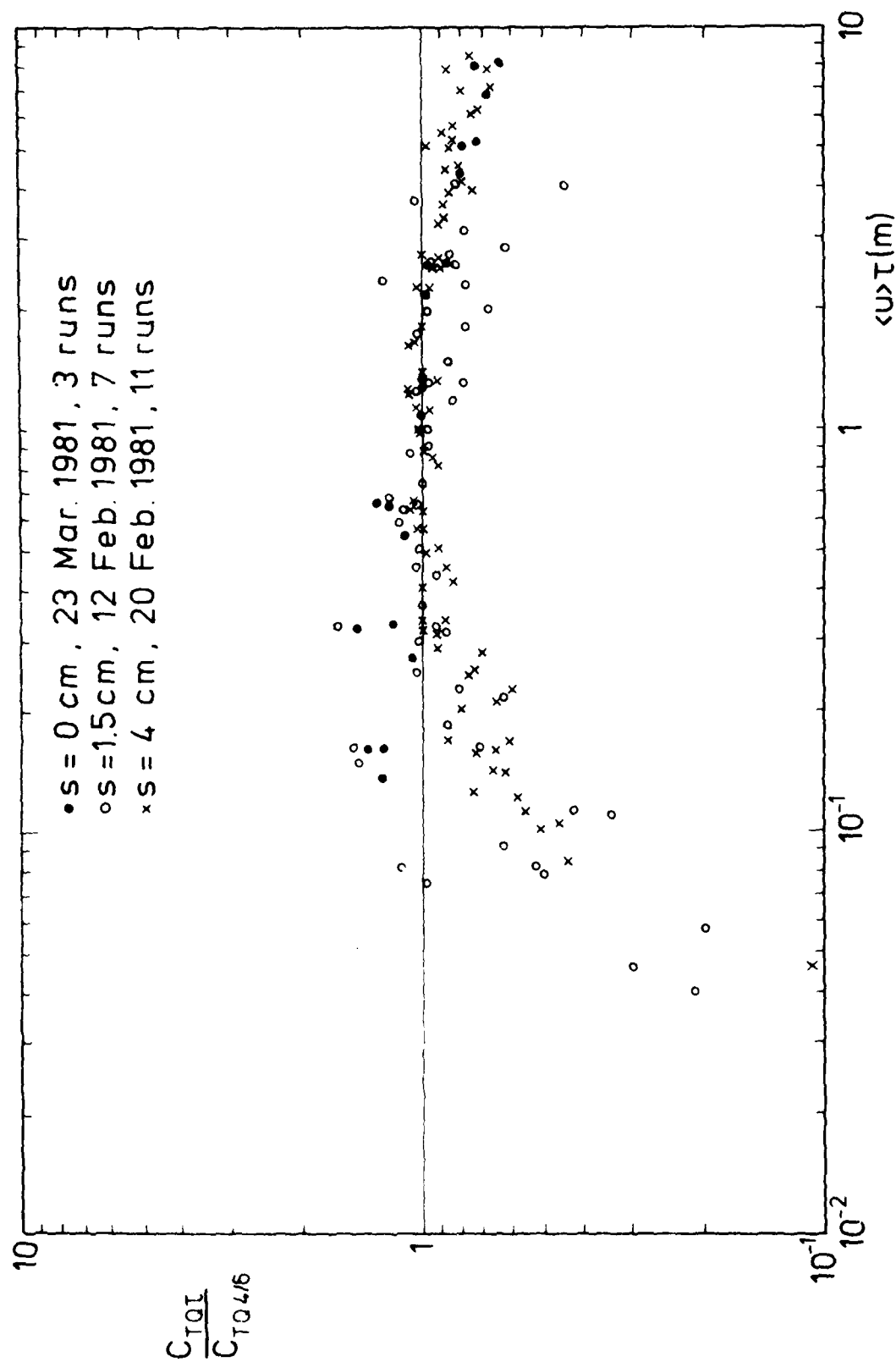
Figure 16.--Time-lagged temperature-humidity structure parameters, normalized to C_{TQ} at specific time lags (C_{TQr} was not measured because of failure of one of the Ly-α's), for various spacings between the temperature and humidity sensors.

42
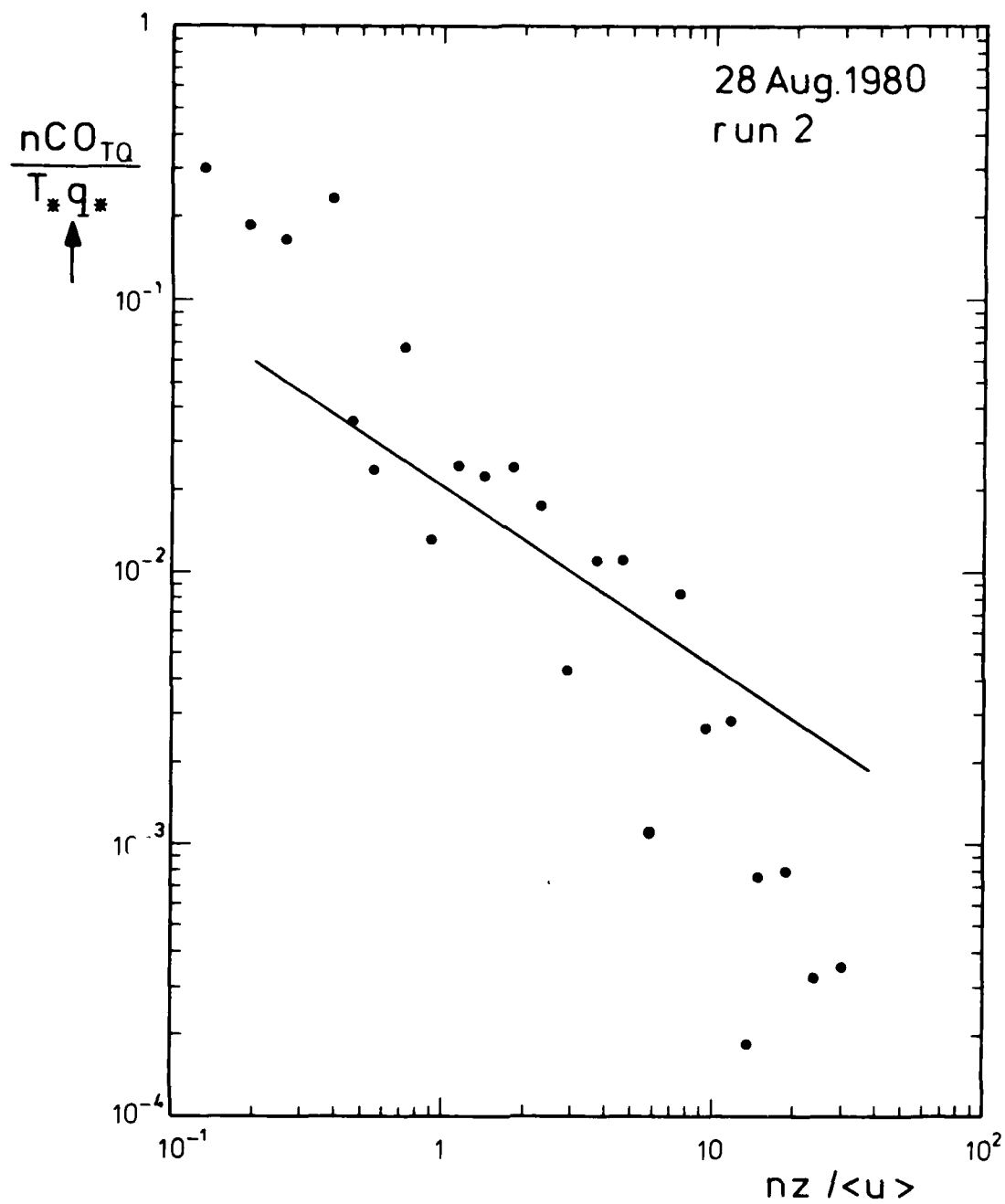
Figure 17.—The normalized temperature-humidity cospectrum. The straight line corresponds to a $n^{-5/3}$ dependency of the cospectrum.

be fitted through the data points for nz/<u> between 1 and 10. At higher values of nz/<u> the cospectrum falls off too rapidly, which can be ascribed to the 4 cm distance between the temperature sensor and humidity sensor. At low values of nz/<u> the cospectrum seems to decrease more rapidly than $n^{-5/3}$ with increasing n, which indicates a rapid decrease of the spectral correlation coefficient.

These observations of the cospectrum neither confirm nor deny the existence of an inertial subrange. Other observations are conflicting. Wyngaard et al., 1978, found an $n^{-5/3}$ behavior from an analysis of the AMTEX data; Friehe et al., 1975, also found $n^{-5/3}$, but they consider their results tentative. Wesely and Hicks (1978) on the contrary, using a step-filter technique, found $n^{-2.2}$. A more rapid decrease of the cospectrum than $n^{-5/3}$ was also observed by McBean and Elliott (1981), but the 0.5 m spacing between their temperature sensor and humidity sensor is likely to have affected the spectrum beyond nz/<u> ∿ 1. Also the mea-surements by Fairall et al. (1980), seem to indicate a more rapid fall-off than $n^{-5/3}$; they believe that this is partly caused by sensor noise.

Finally, we may mention that our observations of C_{TQ} by time-lagging are in support of an inertial subrange for the cospectrum, because they show that $D_{TQ}(r) \sim r^{2/3}$ over almost a decade of r. For instance, using equations (29) and (30), one finds that an n^{-2} cospectrum results in a dependency of $C_{TQ\tau}$ on <u>τ that fits the observations badly (see Fig. 15b).

5.4 Relations Between Structure Parameters and the Turbulent Fluxes of Heat and Water Vapor

We will restrict the discussion to the case of an unstable atmosphere (posi-tive, upward flux of sensible heat). The relations between structure parameters and the fluxes of sensible and latent heat have been discussed by Wyngaard and Clifford (1978). From their expressions (30) and (31) it is easily found that

$$Q_o = \alpha^{-3/4} (C_T^2)^{3/4} \left(\frac{-7 \frac{z}{L_\theta}}{1-7 \frac{z}{L}} \right)^{-1/2} \tag{31}$$

and

$$E_o = \alpha^{-3/4} (C_T{}^2)^{1/4} (C_Q{}^2)^{1/2} \left(\frac{-7 \frac{z}{L_\theta}}{1 - 7 \frac{z}{L}} \right)^{-1/2} , \qquad (32)$$

where

$$\alpha = z^{-4/3} \frac{4}{3} \left(\frac{T}{kg} \right)^{2/3} , \qquad (33)$$

$$L = - \frac{u_*^3 \, T}{kg(Q_o + 0.61 \, TE_o/\rho)} , \qquad (34)$$

$$L_\theta = - \frac{u_*^3 \, T}{kg \, Q_o} . \qquad (35)$$

Here Q_o is the vertical flux of temperature (K m^2 s^{-1}) and E_o that of water vapor (kg m^2 s^{-1}). The quantity u_* is called friction velocity (m s^{-1}); $-\rho u_*^2$ is the vertical flux of momentum. The expression in equations (31) and (32) between parentheses is a stability correction, with L the Monin-Obukhov length including the effect of humidity on buoyancy, and L_θ the same quantity without the humidity effect. The stability correction in (31) has been determined empirically from the Kansas measurements (Wyngaard et al., 1971), but no distinction between L and L_θ was made then. Equation (32) has been proposed in analogy with (31), and is indirectly supported by measurements by Fairall et al., 1980.

We investigated (31) and (32) by plotting $\alpha^{-3/4} (C_T{}^2)^{3/4}/Q_o$ and $\alpha^{-3/4} (C_T{}^2)^{1/4} (C_Q{}^2)^{1/2}/E_o$ versus $-z/L$ (Figs. 18 and 19). The quantities Q_o and E_o were measured by correlating the vertical wind fluctuations with temperature and humidity fluctuations respectively. In calculating α, the "Kansas" value of k, 0.35, was used, and C_T and C_Q were measured with the spaced-sensor technique, or by time lagging, as discussed in the previous sections. The friction velocity u_* was found by using the relations of Dyer and Hicks (1970), assuming $z_o = 0.04$ m (from unpublished measurements by Wyngaard), and k = 0.4 (Wieringa, 1980). In the figures, the stability correction as given in (31) and (32) is indicated; it was calculated putting $L_\theta = L$. (Except for a few runs, the difference between L_θ and L was negligible anyway.) It is seen that this correction is too large; in fact, the data points do not exhibit a clear dependence on stability at all for $-z/L > 2 \times 10^{-2}$.
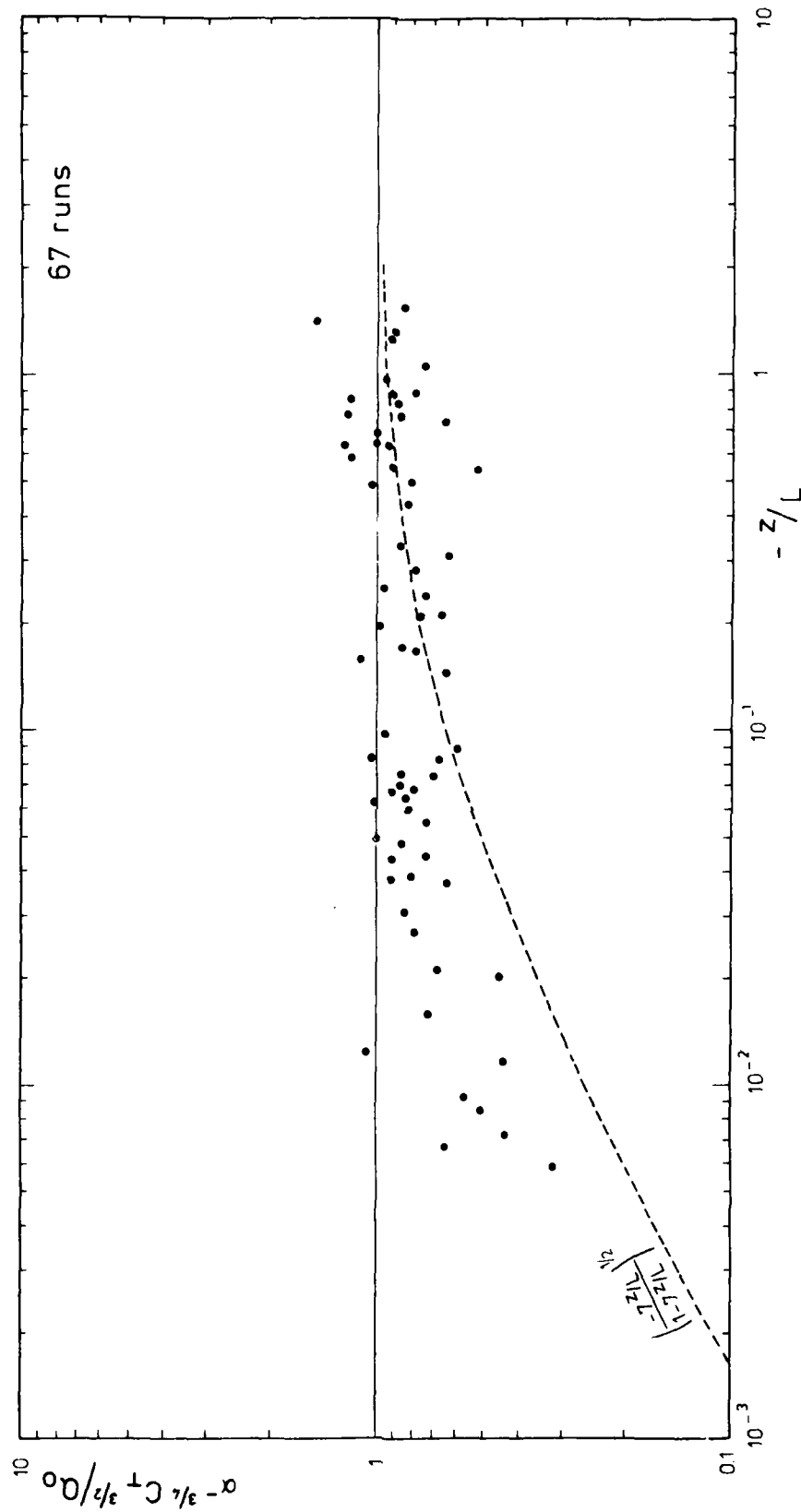
Figure 18.--The free convection prediction of the temperature flux $(\alpha^{-3/4} (c_T^2)^{3/4})$ divided by the observed temperature heat flux $(Q_o = \langle w'T' \rangle)$ as a function of stability $(-z/L)$. The dashed line is the stability dependence according to Wyngaard and Clifford (1978).
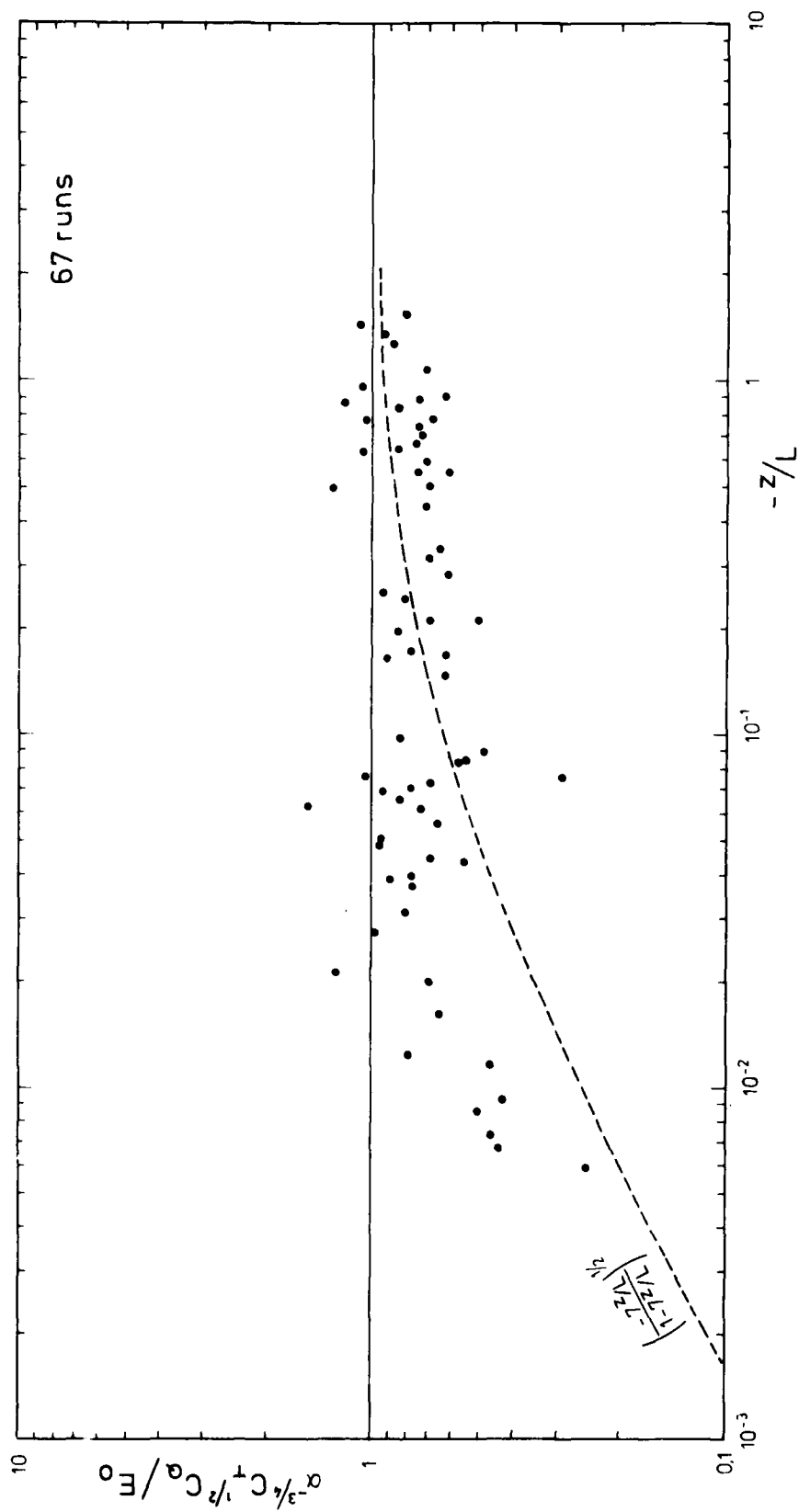
Figure 19.—The free convection prediction of the humidity flux divided by the observed latent heat flux, as a function of stability. Dashed line is stability dependence according to Wyngaard and Clifford (1978).

Also, the observations do not seem to approach the unity line for large $-z/L$, which is most clear for the humidity plot. From these observations, the following relations are suggested:

$$Q_o = \alpha_T^{-3/4} (C_T^{\,2})^{3/4} \; f(-\tfrac{z}{L}) \; , \tag{36}$$

$$E_o = \alpha_Q^{-3/4} (C_T^{\,2})^{1/4} \; (C_Q^{\,2})^{1/2} \; f(-\tfrac{z}{L}) \; , \tag{37}$$

where

$$\alpha_T = 0.83 \, \alpha \quad \text{and} \quad \alpha_Q = 0.74 \, \alpha, \quad \text{and}$$

$$f(-\tfrac{z}{L}) = 1 \qquad \text{for} \qquad -\tfrac{z}{L} > 0.02 \tag{38}$$

$$= \text{decreasing in an undetermined way for}$$

$$0 < -\tfrac{z}{L} \le 0.02 \; .$$

The difference between α and α_T may be non-significant considering the experimental uncertainties, but it is believed that α_Q is definitely somewhat smaller than α. This agrees with observations by Fairall et al. (1980). At $-z/L < 0.02$ there are too few data points, and their scatter is too large to propose a functional relationship to $-z/L$. Why our observations of $(C_T^{\,2})^{3/4}/Q_o$ differ from the Kansas observations for slightly unstable conditions ($-z/L \le 0.2$) is not clear. It should be kept in mind that the Kansas correction may represent these conditions poorly because of the low number of observations there.

The equality of the stability corrections for temperature and humidity fluxes is more clearly demonstrated in Fig. 20, where the ratio of $(C_T^{\,2}/C_Q^{\,2})^{1/2}$ and Q_o/E_o is plotted against $-z/L$. No dependence on stability can be detected. Finally, Fig. 21 gives a plot of $(C_T^{\,2}/C_Q^{\,2})^{1/2}$ versus Q_o/E_o. From these figures it can be concluded that $(C_T^{\,2}/C_Q^{\,2})^{1/2}$ is a very useful estimate of the Bowen ratio (which is directly proportional to Q_o/E_o), independent of atmospheric stability.
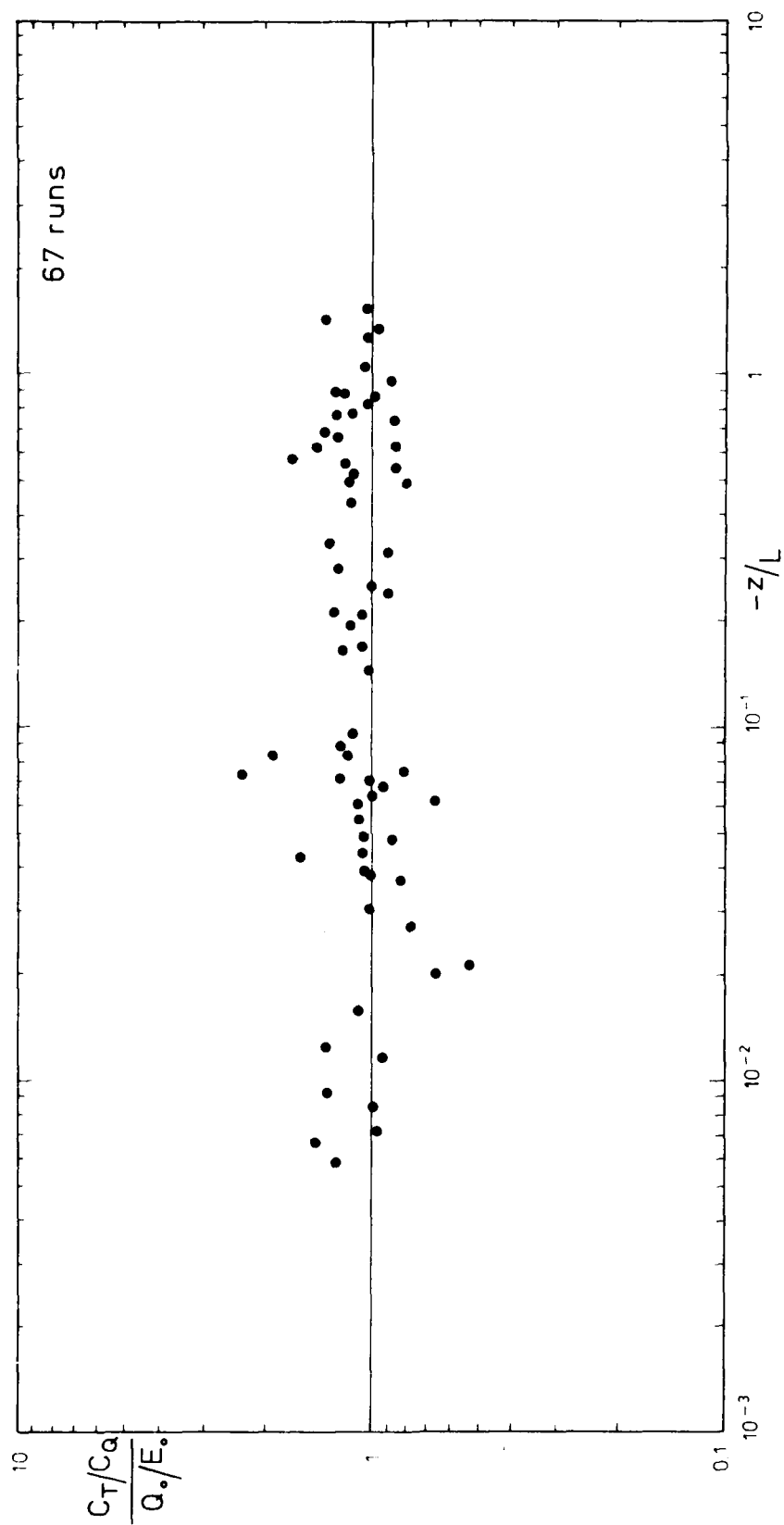
Figure 20.—The ratio of the square roots of the temperature and humidity structure parameter $(C_T{}^2/C_Q{}^2)^{1/2}$ divided by the ratio of the temperature flux and the humidity flux (Q_o/E_o), versus atmospheric stability.
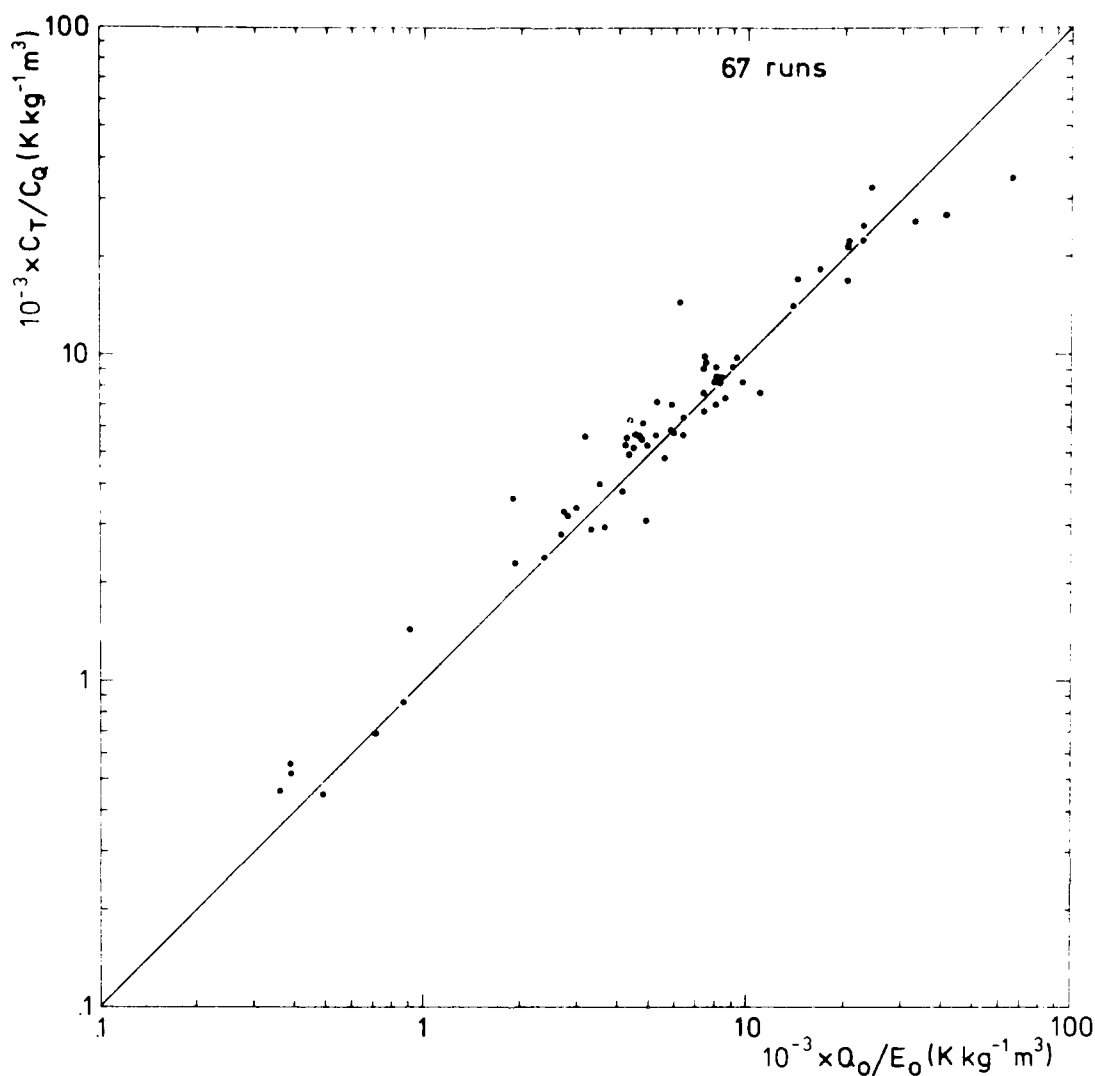
Figure 21.--$(C_T^2/C_Q^2)^{1/2}$ versus Q_o/E_o, which ratio is directly proportional to the Bowen ratio (= sensible heat flux divided by latent heat flux).

6. CONCLUSIONS

The operation of the CO_2 and the HCN scintillometer was hampered by insufficient stability of the pyroelectric detectors; consequently only a few measurements were obtained with the CO_2 scintillometer, and none with the HCN system. Obviously, the application of pyroelectric detectors for these kinds of measurements needs further research. The use of different detectors should be considered, e.g., a HgCdTe detector for the CO_2 receiver, and a bolometer for the HCN receiver. These detectors have to be cooled, which makes the construction of the receiver units more complex.

The LED scintillometer operated satisfactorily, although special attention had to be paid to the calibration of the system. It was found that the transmitter aperture was not completely filled with light, and that there was a net coherence across this aperture.

Experience was gained with Ly-α hygrometers as a tool for measuring C_Q^2 and C_{TQ} (the latter quantity involves measuring both temperature and humidity). Calibration of the Ly-α hygrometer sometimes drifts too much to make such measurements with spatially separated sensors. However, by time-lagging observations of a single sensor, one can also make measurements of C_Q^2 (the equivalent for C_{TQ} is time lagging the observations of a temperature and a humidity sensor that are close together), and this method is not sensitive to drift of the Ly-α hygrometer. Therefore, the time-lagging technique is to be preferred to the spatially separated sensors technique for the measuring of C_Q^2 and C_{TQ}.

By changing the time lag, the equivalent distance between the points of observation (defined as the product of the time lag τ and the wind speed $\langle u \rangle$) may be varied. In this way the dependency of the structure parameter on distance ($\langle u \rangle \tau$) was checked. C_T^2 proved to be independent of $\langle u \rangle \tau$, for 0.01 m < $\langle u \rangle \tau$ < 1 m (0.01 m is no lower limit, but just the smallest distance observed). C_Q^2 was constant for 0.1 m < $\langle u \rangle \tau$ < 2m, and C_{TQ} was constant for 0.3 m < $\langle u \rangle \tau$ < 3 m. The drop-off of C_Q^2 for $\langle u \rangle \tau$ < 0.1 m could not be explained. The drop-off of C_{TQ} at $\langle u \rangle \tau$ < 0.3 m is likely to be caused by the 4 cm separation between the humidity and temperature sensors. It is noted that there still is no complete understanding of the response characteristics of a Ly-α hygrometer.

The power spectra of temperature and humidity, and the temperature-humidity cospectrum were calculated for several runs of approximately 15 minutes duration. An inertial subrange was found for the power spectra. For the cospectrum, however, a definite inertial subrange behavior could not be established because of considerable scatter of the data in the limited frequency interval available. From the link between the dependency of a spectrum on wavenumber on the one hand, and the dependency of the structure function on distance on the other, it may be concluded that the cospectrum should have an inertial subrange as well.

The relations between the structure parameters $C_T{}^2$ and $C_Q{}^2$, and the vertical fluxes of temperature (Q_o) and humidity (E_o) for an unstable atmosphere were investigated. The free convection predictions worked very well, not only for very unstable conditions, but also down to $-z/L \sim 0.02$. The constant of proportionality between E_o and $[(C_T{}^2)^{1/2} C_Q{}^2]^{1/2}$ is found to be about 10% less than that between Q_o and $(C_T{}^2)^{3/4}$. For arbitrary instability, the ratio $(C_T{}^2/C_Q{}^2)^{1/2}$ is a very useful measure of the Bowen ratio (that is, of the sensible heat flux divided by the latent heat flux).

7. ACKNOWLEDGMENTS

8. REFERENCES

Andreas, E.L., 1981: The effects of volume averaging on spectra measured with a Lyman-alpha hygrometer. J. Appl. Meteorol., 20, 467-475.

Belland, P., and D. Véron, 1973: A compact CW HCN laser with high stability and power output. Optics Comm., 9, 146-148.

Belland, P., Véron, D., and L.B. Whitbourn, 1976: Scaling laws for CW 337-μm HCN waveguide lasers. Appl. Optics, 15, 3047-3053.

Buck, A.L., 1977: Lyman-alpha radiation source with high spectral purity. Appl. Optics, 16, 2634-2636.

Buck, A.L., 1980: RSF/RAF Lyman-alpha hygrometer model LA-3. Operating and maintenance manual 083-032-007, National Center for Atmospheric Research, Boulder, Colo.

Corrsin, S., 1951: On the spectrum of isotropic temperature fluctuations in an isotropic turbulence. J. Appl. Phys., 22, 469-473.

Coulter, R.L., and M.L. Wesely, 1980: Estimates of surface heat flux from sodar and laser scintillation measurements in the unstable boundary layer. J. Appl. Meteorol., 19, 1209-1222.

Davidson, K.L., Houlihan, T.M., Fairall, C.W., and G.E. Schacher, 1978: Observation of the temperature structure function parameter, C_T^2, over the ocean. Boundary-Layer Meteorol., 15, 507-523.

Dyer, A.J., and B.B. Hicks, 1970: Flux-gradient relationships in the constant flux layer. Q. J. R. Meteorol. Soc., 96, 715-721.

Fairall, C.W., Schacher, G.E., and K.L. Davidson, 1980: Measurements of the humidity structure function parameters, C_q^2 and C_{Tq}, over the ocean. Boundary-Layer Meteorol., 19, 81-92.
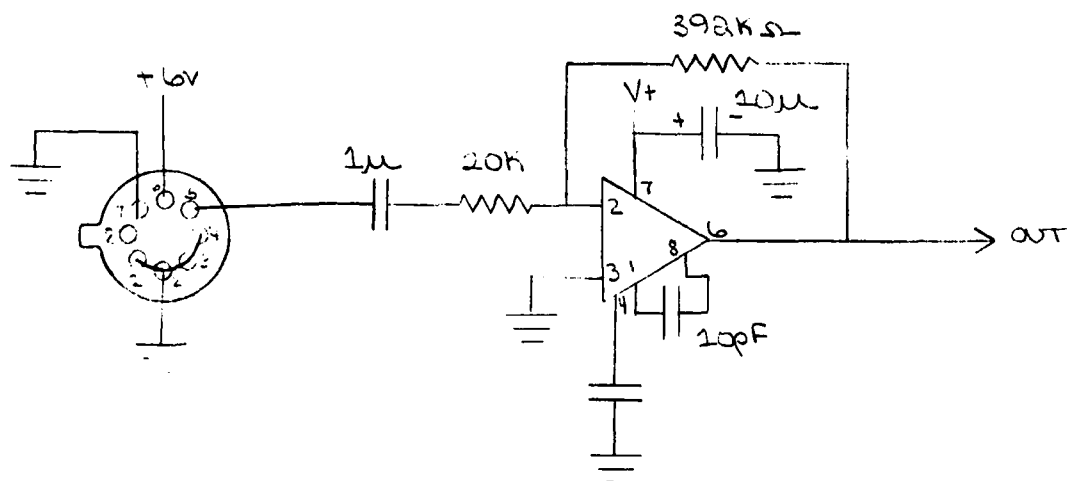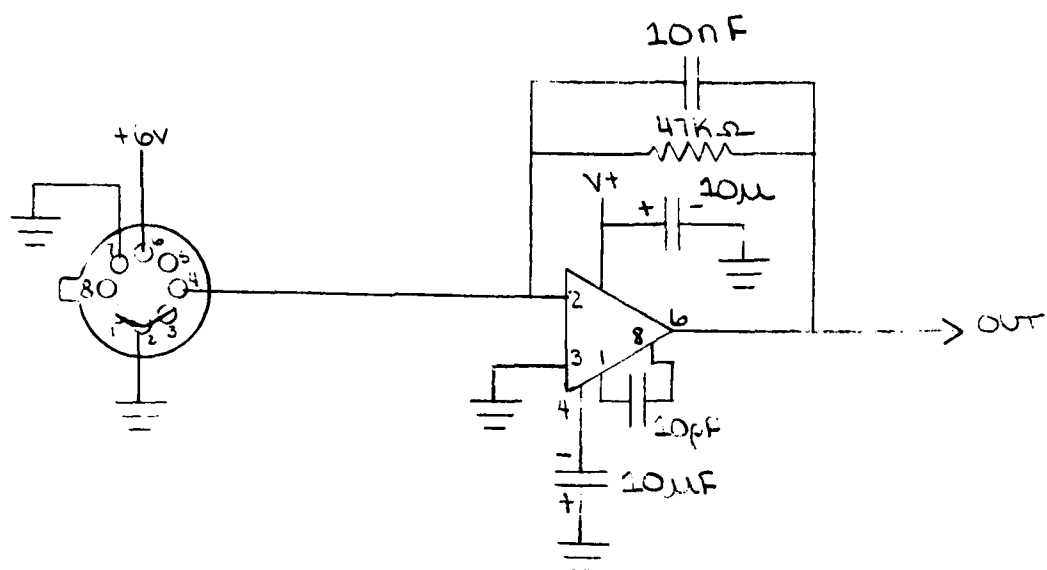
Friehe, C.A., LaRue, J.C., Champagne, F.H., Gibson, C.H., and G.F. Dreyer, 1975: Effects of temperature and humidity fluctuations in the optical refractive index in the marine boundary layer. J. Opt. Soc. Am., 65, 1502-1511.

Hill, R.J., 1978a: Spectra of fluctuations in refractivity, temperature, humidity, and the temperature-humidity cospectrum in the inertial and dissipation ranges. Radio Science, 13, 953-961.

Hill, R.J., 1978b: Models of the scalar spectrum for turbulent advection. J. Fluid Mech., 88, 541-562.

Hill, R.J., and S.F. Clifford, 1978: Modified spectrum of atmospheric temperature fluctuations and its application to optical propagation. J. Opt. Soc. Am., 68, 892-899.

Hill, R.J., and G.R. Ochs, 1978: Fine calibration of large-aperture optical scintillometers and an optical estimate of inner scale turbulence. Appl. Optics, 17, 3608-3612.

Hill, R.J., Clifford, S.F., and R.S. Lawrence, 1980: Refractive-index and absorption fluctuations in the infrared caused by temperature, humidity and pressure fluctuations. J. Opt. Soc. Am., 70, 1192-1205.

McBean, G.A., and J.A. Elliott, 1981: Pressure and humidity effects on optical refractive-index fluctuations. Boundary-Layer Meteorol., 20, 101-109.

Ochs, G.R., Cartwright, W.D., and D.D. Russell, 1980: Optical C_n^2 instrument model II. NOAA Technical Memorandum ERL WPL-51.

Tillman, J.E., 1965: Water vapor density measurements utilizing the absorption of vacuum ultraviolet and infrared radiation. In: Humidity and Moisture, Vol. I, Arnold Wexler, Ed., Rheinhold Publishing Corp., New York.

Wang, Ting-i, Ochs, G.R., and S.F. Clifford, 1978: A saturation-resistant optical scintillometer to measure C_n^2. J. Opt. Soc. Am., 68, 334-338.
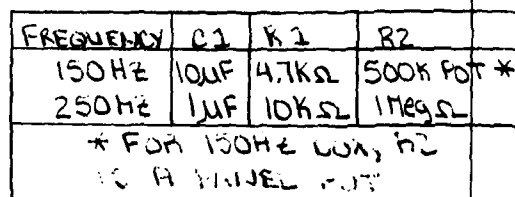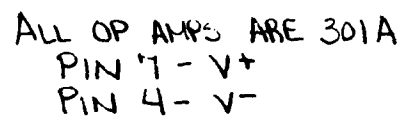
Wells, J.S., Evenson, K.M., Matarrese, L.M., Jennings, D.A., and G.L. Wichman, 1971: Design for a variable-output-coupling far-infrared Michelson laser. NBS Technical Note 395.

Wesely, M.L., 1976: The combined effect of temperature and humidity fluctuations on refractive index. J. Appl. Meteorol., 15, 43-49.

Wesely, M.L., and B.B. Hicks, 1978: High-frequency temperature and humidity correlation above a warm wet surface. J. Appl. Meteorol., 17, 123-128.

Wieringa, J., 1980: A revaluation of the Kansas mast influence on measurements of stress and cup anemometer overspeeding. Boundary-Layer Meteorol., 18, 411-430.

Wyngaard, J.C., Izumi, Y., and S.A. Collins, Jr., 1971: Behavior of the refractive-index-structure parameter near the ground. J. Opt. Soc. Am., 61, 1646-1650.

Wyngaard, J.C., 1973: On surface-layer turbulence. Workshop on Micrometeorology, Amer. Meteorol. Soc., 101-149.

Wyngaard, J.C., and S.F. Clifford, 1977: Taylor's hypothesis and high-frequency turbulence spectra. J. Atmos. Sci., 34, 922-929.

Wyngaard, J.C., and S.F. Clifford, 1978: Estimating momentum, heat and moisture fluxes from structure parameters. J. Atmos. Sci., 35, 1204-1211.

Wyngaard, J.C., Kaimal, J.C., Ochs, G.R., Hill, R.J., and D.C. Sorensen, 1978: An optical heat flux experiment. Preprints 4th Symp. Meteorological Observations and Instruments, Denver, Amer. Meteorol. Soc., 47-50.

APPENDIX I

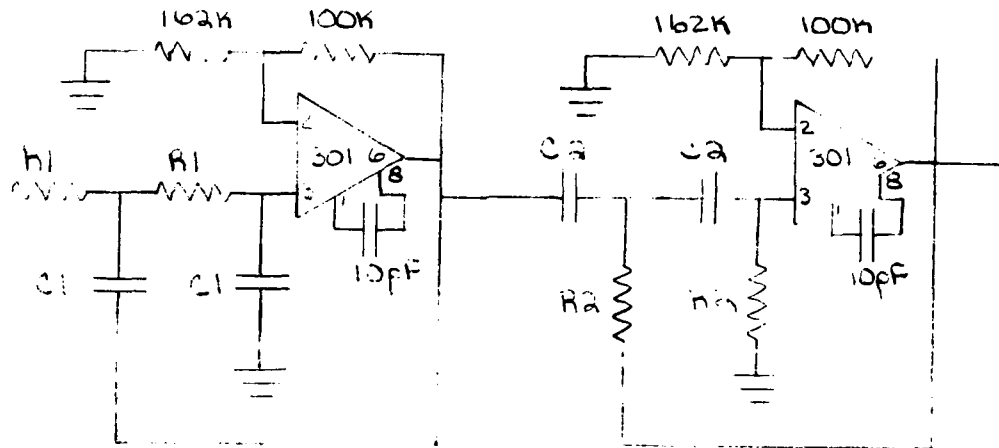THE CO$_2$ AND HCN SCINTILLOMETER ELECTRONICS

DETECTOR AMPLIFIER.

10nF

47KΩ

V+
10μ

2
3
8
6
4
10pF

10μF

OUT

+6V

392KΩ

V+
10μ

1μ   20K

2
3
8
6
4
10pF

OUT

+6V

ALL OP AMPS ARE 301A
PIN 7 - V+
PIN 4 - V-

FREQUENCY	C1	R1	R2
150 Hz	10μF	4.7kΩ	500k POT *
250 Hz	1μF	10kΩ	1MegΩ

* FOR 150Hz LOX, R2
IS A PANEL POT

AUTOMATIC GAIN CONTROL CIRCUIT

BAND-PASS FILTER

	R1	C1	R2	C2
150Hz	18.2KΩ	.047μF	13.3KΩ	.1μF
250Hz		.022μF		.022μF

ALL 301 OP-AMPS
  PIN 4 = -V
  PIN 7 = +V

APPENDIX II

THE Ly-α ELECTRONICS
(after Buck, 1980)
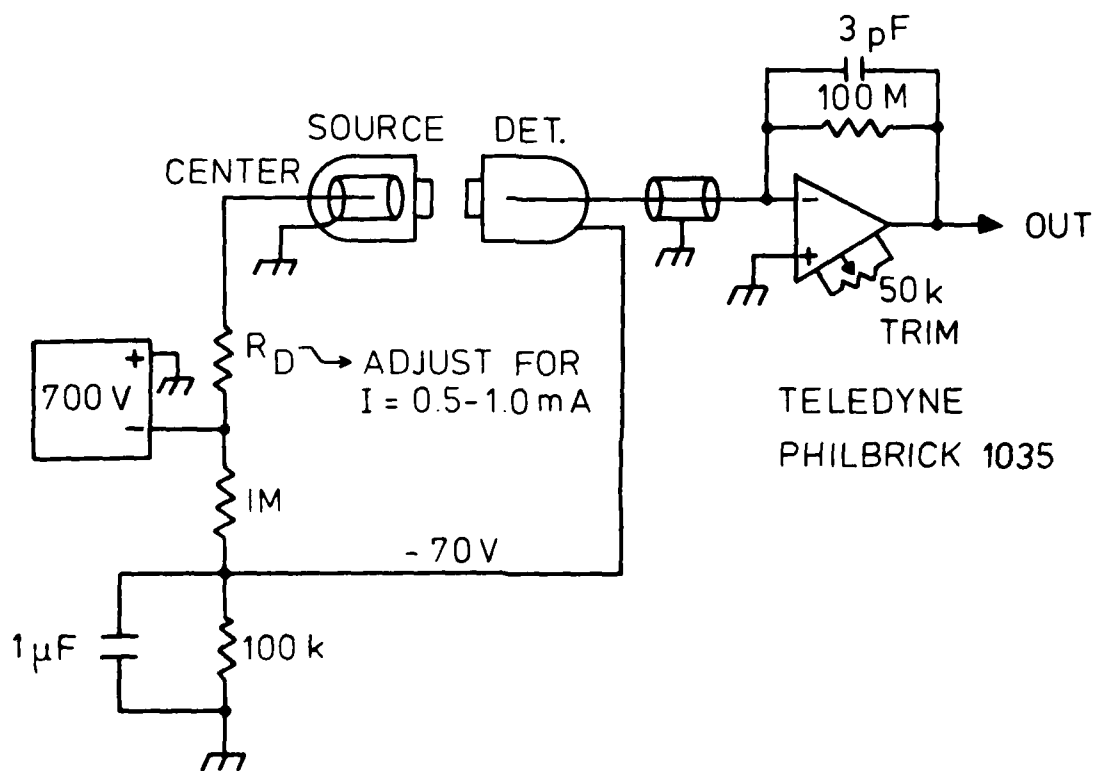
APPENDIX III

EFFECT OF UNEQUAL Ly-α HUMIDITIES ON THE MEASUREMENTS OF C_Q^2 AND C_{TQ}

1. The humidity structure function

The humidity structure function D_Q is calculated with

$$D_Q = <(A-B)^2> - <A-B>^2 , \tag{III-1}$$

where the measured humidities are denoted by A and B. Now, let us suppose that humidity A is correct, but B is off by a factor $(1+\delta)$:

$$B = (1+\delta)B* , \tag{III-2}$$

$$<B*> = <A> , \tag{III-3}$$

$$<B*^2> = <A^2> . \tag{III-4}$$

Inserting these expressions in Eq. (III-1), one finds the observed structure function D_Q^{obs}:

$$D_Q^{obs} = (1+\delta)[2<A^2> - 2<AB*>] + \delta^2[<A^2> - <A>^2] .$$

The true structure function is

$$D_Q^{true} = <(A-B*)^2> - <A-B*>^2 = 2<A^2> - 2<AB*> , \tag{III-5}$$

so the ratio of the observed to the true structure parameter is

$$\frac{D_Q^{obs}}{D_Q^{true}} = 1+\delta + \delta^2 \frac{v_Q}{D_Q^{true}} , \tag{III-6}$$

where v_Q denotes the variance of the humidity ($= <A^2> - <A>^2$). The ratio v_Q/D_Q^{true} generally depends on the distance between the two humidity sensors, and it can be quite high--10 or more. The term with δ^2 may thus contribute significantly, even at a low value of δ. In practice, it is wise to have δ not larger than a few percent.

2. The temperature-humidity structure parameter

The quantity is defined by

$$D_{TQ} = \langle (T_A - T_B)(Q_A - Q_B) \rangle \ .$$

<div align="right">(III-7)</div>

It is supposed that $\langle T_A - T_B \rangle = 0$ (forced by high pass filtering). Following the same line of reasoning as in the foregoing section we find

$$\frac{D_{TQ}^{obs}}{D_{TQ}^{true}} = 1 - \delta \ \frac{\langle (T_A - T_B)Q_B^* \rangle}{D_{TQ}} \ ,$$

<div align="right">(III-8)</div>

where Q_B^* is the corrected value of humidity sensor B, so that $\langle Q_B^* \rangle = \langle Q_A \rangle$, etc. We have no observed values of $\langle (T_A - T_B)Q_B^* \rangle$ available. An upper estimate of (III-8) is obtained if we suppose $\langle T_A Q_B^* \rangle \ll \langle T_B Q_B^* \rangle$; then

$$\frac{D_{TQ}^{obs}}{D_{TQ}^{true}} \approx 1 + \delta \ \frac{\langle T_B Q_B^* \rangle}{D_{TQ}} = 1 + \delta \ \frac{r_{TQ}\sigma_T \sigma_Q}{D_{TQ}} \ .$$

<div align="right">(III-9)</div>

Here σ_r and σ_Q are the standard deviations of the temperature and humidity, respectively. The quantities on the right in (III-9) all have been measured. It was found that the multiplier of δ may be up to 10 with a spacing of 0.31 m between the sensor pairs A and B. Although Eq. (III-9) is surely an overestimate , it is clear that in the case of the measurement of D_{TQ} it is wise to have δ not larger than a few times a hundredth.

END

DATE
FILMED

5-82

DTIC